TAMPEREEN TEKNILLINEN YLIOPISTO
TAMPERE UNIVERSITY OF TECHNOLOGY

MOHAMMAD HOSSAIN

IMPLANTED WIRELESS SENSORS FOR MEDICAL APPLICATIONS: EXPLORING THE LIMITS OF INDUCTIVE POWERING

Master of Science Thesis

Examiner:
Toni Björninen
Muhammad Waqas Ahmad Khan
Examiners and topic approved by the Computing and Electrical Engineering faculty council on 29 March 2017

ABSTRACT

MOHAMMAD HOSSAIN: Implanted Wireless Sensors For Medical Applications: Exploring the Limits of Inductive Powering.
Tampere University of technology
Master of Science Thesis, 49 pages, 2 Appendix pages
June 2017
Master's Degree Programme in Electrical Engineering
Major: Electronics Engineering
Examiner: Toni Björninen, and Muhammad Waqas Ahmad Khan

Keywords: Wireless power transfer, Inductive powering, Wearable antenna, Spiral circular antenna, Link power efficiency, Specific absorption rate.

Wireless medical implant powering is an emerging sector for future healthcare applications. It enhances the healthcare safety level and the prospects of a better life. The main theme of this research is to design a wireless power budgeting for the medical implants. A proper link between an external source to the implant is established by an inductive coupling for a particular physiological parameter monitoring. A battery-free implant device requires sufficient power supply for active monitoring.

The main target of this research is to develop a wearable and external antenna design for transferring sufficient power to the implant for its activation without violating the regulations of specific absorption rate limits. In addition, there is another goal of improving the implant depth. In this research, two different models (link model and SAR model) are used for the assessment in the virtual environment. Previously, a two-turns antenna is used for power transmission but in this research, several antenna structures are studied such as – the circular two-turns with a capacitor loaded loop, benzene shape, rectangular shape, octagonal shape, and circular spiral shape. Among these structures, circular spiral shape, with the combination of same and counter directions of spiral loops, shows satisfactory results. Through the proper optimization approach, the circular spiral antenna is capable of providing 25% more power at the implant with respect to the two-turns antenna. For 16 mm link distance, the circular spiral antenna can transmit 686 mW whereas a two-turns antenna is efficient up to 452 mW. Even the implant can be placed 2.5 mm more depth without interrupting the power transmission link between antennas. The circular spiral antenna is able to transfer significant power up to 9 mm skull thickness whereas 6.4 mm is the average width.

Two experimental setups are developed for antenna performance analysis such as "*air gap testing*", and "*pigskin and air gap testing*". In the experiments, the effect of parasitic elements over the link power efficiency is identical to both the experiments. The results of "*in vitro*" testing of the newly developed wearable external antenna inspires for future implementation in the monitoring of intracranial pressure. From the performance analysis, in both the virtual environment and experimental setup, the circular spiral antenna has enough potentiality to use in inductive powering for further research and development.

PREFACE

It was a long and hard working journey, however; I really enjoyed this period. I started my thesis work in November 2016, after my ACL reconstruction surgery. Initially, it was difficult for me to emphasis my full concentration in thesis work because of physical issues but I geared up my working speed in December during my rehabilitation period.

This thesis work was performed at the “Wireless Identification and Sensing Systems Research Group (WISE)” at the Department of Electronics and Communications Engineering in the Tampere university of Technology (TUT), Finland. At the beginning, I divided the whole thesis into different tasks including specific time duration. I would like to thank my supervisors (Toni Björninen and M. Waqas A. Khan) because they supported me to complete the thesis work in appropriate time. They guided me properly in the right direction. I learned new simulation and experimental tools from them. Overall, I really enjoyed this research. I always thought that I was learning something new in every day.

I also want to thank my colleagues at the Tampere University of technology for their valuable comments or suggestions about my thesis and future planning. I would like to thank Aminul Jony, Sharmin Sultana Himi, Tutul Rozario, Tushar Sarker, Mahabub Rubel, and my sister Afia Maheda Prema for their mental support. During my thesis probably, I passed the most difficult part of life but they always supported me. Special thanks to my parents for their guidance in every stage of my life. I want to remember my beloved late grandfather. At the end, my final thanks go to Fatema Tuz Zohura Lopa for her love and words of encouragement.

Mohammad Akter Hossain

Tampere, 24.5.2017

CONTENTS

LIST OF FIGURES

LIST OF TABLES

LIST OF ABBREVIATIONS

ICP	Intracranial pressure
CSF	Cerebrospinal fluid
RF	Radio Frequency
U.S FCC	Federal Communications Commission (USA)
SAR	Specific absorption rate
ANSYS HFSS	Simulation software for High Frequency Electromagnetic Field
WPT	Wireless Power Transfer
RFID	Radio Frequency Identification
TX	Transmitter
RX	Receiver
IC	Integrated Circuit
DC	Direct Current
IEEE	Institute of Electrical and Electronics Engineers
UV	Ultra-Violate
PCB	Printed Circuit Board
VNA	Vector Network Analyzer
SMA	Sub-Miniature Version A

LIST OF SYMBOLS

P_{tmax}	Maximum transferred power
P_L	Power at implant's load
G_{Pmax}	Link power efficiency
G_P	Transducer gain
μ_0	Permeability in the vacuum
$\vec{H}$	Magnetic flux density
I, i	Current
L	Length
$\overrightarrow{dl}$	Small amount of length
R	Radius
Θ	Theta, used to denote the angle
Φ_B	Magnetic flux
A	Area
$d\vec{A}$	Small amount of area
$\vec{E}$	Electromagnetic field
dt	Time
Z_S	Source impedance
Z_L	Load impedance
Z_{IC}	IC impedance
C	Capacitor
L	Inductor

P	Power
ω	Angular frequency
N	Number of turns
V_{ind}	Induced voltage
P_t	Simulation test power
τ_{S-ta}	Power transmission coefficient between source and transmitting antenna
A_V	Voltage gain
V_{in}	Voltage amplitude at the transmitting antenna
V_L	Voltage amplitude at IC
τ_{S-ta}	Power transmission coefficient between input impedance and IC input impedance
d_{im}	Inductive link distance

1. INTRODUCTION

Wireless power transfer by inductive coupling is used for the portable devices, gadgets, and in healthcare applications such as medical implant powering. It improves the healthcare safety level as well as the prospects of a better life. The wireless power transfer would provide an innovative way of intracranial pressure (ICP) monitoring. In 1783, Alexander Monroe introduced the notion of intracranial pressure [1]. After some years, George Kellie performed few experiments and bolstered Monroe's concept [2]. According to the principle of Monroe-Kellie, the cranial cavity consists of three basic elements – blood, cerebrospinal fluid (CSF) and brain [3],[4],[5].

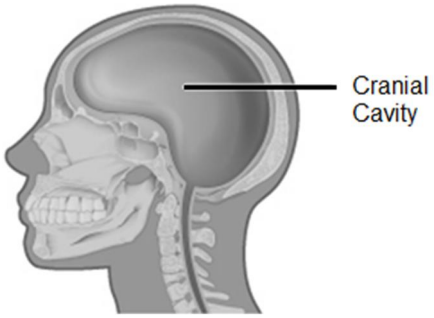

Figure 1. *Cranial cavity of a human head.*

Figure 1 is representing the side view of the cranial cavity of a human head. The area of the cranial cavity is restrained by its structure and the existing elements inside of it are volume equilibrium. However, different injuries or disorders may disturb the equilibrium state of existing element's volume in the cranial cavity. If the volume of one element increases accidentally, then other two elements are unable to compensate for volume change within a fixed area. In this circumstance, the increased volume with a fixed area causes a higher pressure to the surroundings. For adult human, 7 mmHg to 15 mmHg is the normal range of ICP [6]. Nevertheless, due to injury or disorder, the upper limit of ICP may rise above 20 mmHg [3],[4],[5]. The most common result due to the raised ICP is ischaemia. Ischaemia means the inadequate blood supply to brain tissues. The restriction of blood supply causes the deficiency of oxygen and glucose in the tissues. Oxygen and glucose are highly demandable for cellular metabolism that keeps the tissue alive. Eventually, ischaemia develops without intervention to infarction (cell death) which may cause irretrievable brain damage and turns to often lethal. To avoid any critical damage to the brain, the targeted level of ICP is to keep within 20 mmHg [3],[4],[5].

Although external ventricular drainage is a method of the ICP monitoring with high accuracy but this process is invasive and patients are unable to move in a comfortable way. A catheter is inserted into the ventricular system of the brain through a burr hole. The invasive ICP monitoring process has a high risk of infection and hemorrhage [3],[4],[5],[8]. This process is not optimal for long-term monitoring [9]. However, a minimally invasive implanted sensor may overcome these drawbacks by maintaining a satisfactory level of accuracy [8],[10]. Implanted pressure sensing system is proposed for long-term monitoring of ICP. Previously developed research approaches have some shortcoming such as the sensitivity of the capacitive pressure sensors system [11],[12],[13],[14] and power budget management [11]. However, an implanted wireless sensor system reduces the complexity of battery issues. Instead of using the battery in the implant, the inductive wireless power transmission is introduced [15],[16]. The required power is transferred from an external device to the implant. Previously, a two-turns antenna is used for wireless power transmission [15],[16].

The main objective of this research is to improve the existing external antenna design [15]. A new external antenna design is developed to improve the link distance. In addition, it is necessary to evaluate the maximum level of implant depth by keeping the implant in active mode. In this research, two different models are used for assessment in the virtual environment. Those models are – link model and SAR model. In an inductive link, the gain describes the power transfer efficiency between the antennas. The gain of the antenna is measured by the link model. Biological tissues can absorb electromagnetic energy when the source of this energy is exposed in front of those tissues. SAR is the rate of energy absorption by the human body when exposed to RF electromagnetic field. According to the regulations of U.S. FCC, the safety margin of SAR should be less than 1.6 W/kg [15]. On the surface, the skin tissues are relatively close to the transmitting antenna with respect to other internal tissues and skin tissues absorb the maximum electromagnetic energy as well as it has maximum SAR values. The relationship between electromagnetic energy and SAR is directly proportional. Moreover, if the SAR is higher, the maximum amount of power is absorbed in tissue layers instead of transmitting sufficient power to the implant. This phenomenon leads lower transmitting power (P_{tmax}) and lower power at implant's load (P_L). However, an external inductive loop antenna with good link power efficiency (G_{tmax}) has a high Electric field near the feed point, which may lead the increment of SAR values. Therefore, this is a tradeoff approach between gain and SAR to get an optimal performance [15].

Beforehand, a two-turns antenna is used for power transmission [15] but in this research, several antenna structures are studied such as - circular two-turns with a capacitor loaded loop, benzene shape, rectangular shape, octagonal shape, circular spiral shape. The optimally performed antenna is chosen for fabrication. The performance of the existing two-turns antenna is taken as the reference for comparison. Among these structures, circular spiral shape, with the combination of same and counter directions of spiral loops, initially

shows satisfactory results. After that, the dimensions of the circular spiral antenna have optimized. The performance of two-turns antenna and circular spiral antenna is compared in three different studies such as – implant depth, skull thickness variation, and the variation of external antenna distance and implant depth from the skin. A couple of studies have been done to evaluate the maximum link distance. In both cases, the position of the external antenna is fixed but implant depth or skull thickness is increased and thus the link distance is increased. The maximum implant depth or maximum skull thickness for the circular spiral antenna can be observed when the antenna can transmit the same amount of power of the two-turns antenna for the further increment of link distance. These studies are made in the virtual environment by using ANSYS HFSS.

After simulation, the circular spiral antenna is fabricated including a matching circuit. Then in vitro testing does the final performance evaluation. Inductive powering from the external antenna to the implant antenna is practically tested in this stage. Initially, this test of inductive powering is done in the air medium. Secondly, 6 mm pigskin is introduced within the air medium for another experimental setup. From the performance analysis, in both the virtual environment and experimental setup, the circular spiral antenna has enough potentiality to use in inductive powering for further research and development.

The thesis consists of six chapters. Chapter 1 provides a short introduction to wireless power transmission by inductive coupling, its application in the medical field and the main objectives of the thesis. Chapter 2 describes the theoretical background of the thesis. The concept of wireless power transfer by inductive coupling for implant biotelemetry and wireless link modelling are briefly explained. Chapter 3 discusses the existing antenna, the evolution of the antenna structure and optimization of the antenna with the variation between spacing and thickness. Chapter 4 provides a brief overview of the performance comparison between two turns and spiral circular antenna. Chapter 5 presents the experimental setups and measurement. The process of antenna fabrication and the matching circuit are briefly explained. Simultaneously, the performance of the circular spiral antenna is analyzed by two "*in vitro*" experimental setup - "*air gap testing*", and "*pigskin and air gap testing*". The final chapter summarizes the most important outcomes of the entire thesis work and future prospects.

2. LITERATURE REVIEW

Wireless inductive powering and wireless link modeling are the main highlighting points of this chapter. Those are divided into two sections. In Section 2.1, the notion of wireless power transfer is discussed briefly. Nevertheless, this thesis is an application of near-field inductive powering. Section 2.1 is divided into two subsections. Subsection 2.1.1 presents the conventional theories of physics. Moreover, the method of inductive powering is more emphasized in 2.1.2 subsection. In Section 2.2, wireless link modeling through the inductive way are discussed. It has two subsections; one subsection discusses about the theory of the two-port network and another subsection discusses the scientific background and the equations for the simulation process.

2.1 Wireless power transfer

Wireless power transfer (WPT) is an innovative way of power transmission from the source to desired load destination without any direct connectivity between them. Nikola Tesla, the father of wireless charging, invented the idea of WPT [17]. In modern civilization, WPT is widely used for portable devices and gadgets such as medical implant powering [18]. WPT can be achieved by three technologies for instance induction coupling, microwave power transmission. These three technologies can be categorized under two techniques. Induction coupling and resonance coupling are under near-field technique and microwave power transmission is under far-field technique [17].

2.1.1 Basic concept of inductive power transfer

In 1888, Heinrich Hertz observed and verified the notion of inductive powering. He performed an experiment where he created a spark gap between transmitter and receiver with the help of electromagnetic waves [17]. In the concept of inductive powering which is illustrated in Figure 2, there are two separate coils – transmitter and receiver coil. When, an electric current is passed through one coil then it produces a short-range magnetic field. If the second coil is placed near to the first coil, within that short magnetic field range, then an electric current pass through the second coil. There is no direct contact between first and second coil. Energy is transferred through mutual induction.

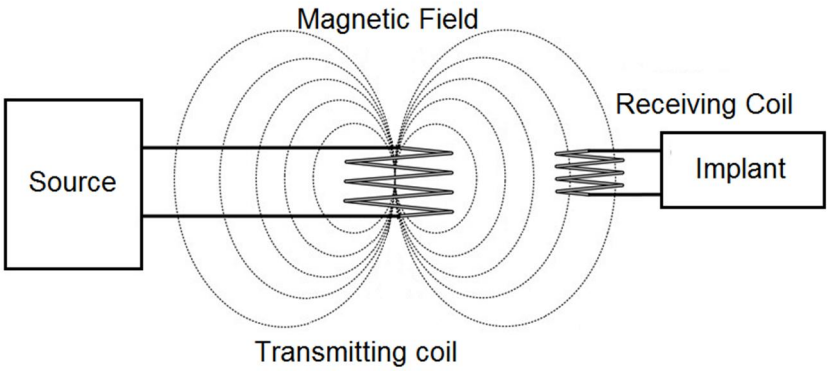

Figure 2. *Fundamental illustration of inductive power transfer.*

The main principle of inductive powering is based on Ampere's circuital law and Faraday's induction law [18],[19],[20],[21]. These laws are the part of Maxwell's equations [22],[23]. In 1826, Ampere was doing research on electric current behavior in a wire [20]. At the same time, Faraday was also doing an experiment for his laws of induction [20]. However, later Maxwell did some extension of Ampere's law and incorporated those theories.

According to Andre Marie Ampere, the loop integral of a magnetic field is equal to the product of permeability in a vacuum and enclosed current in the loop.

$$\oint \vec{H}.\vec{dl} = \mu o * i \tag{1}$$

where, μ_0 is the permeability in the vacuum (μ_0= 4.$\boldsymbol{\pi}$.10^{-7} H/m), $\vec{H}$ is magnetic field which is generated by electric current flowing through the wire and *dl* is the small segment of arbitrary path length. If the arbitrary path is circular then the total length is $2.\boldsymbol{\pi}.r$. Field and current flow direction are determined by right-hand rule.

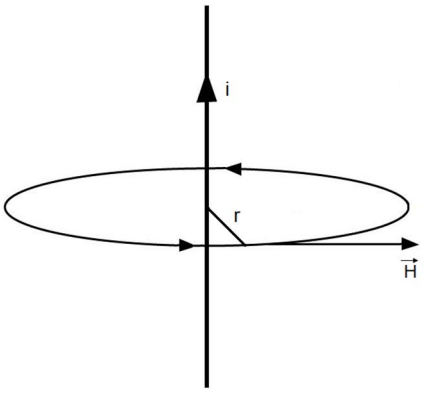

Figure 3. *Illustration of Ampere's law.*

From equation 1,

$$2 * \pi * r * H = \mu o * i \quad (2)$$

And for a constant electric current,

$$H \propto \frac{1}{r} \quad (3)$$

Equation 3 states that the value of a magnetic field is decreased with an increase of the radius of an arbitrary path from a wire.

The magnetic field can also get from Biot-Savart law. In Figure 4, if the current i flow through a wire and wire is divided into the small segment $\overrightarrow{dl}$ then each segment develops a magnetic field. The cumulative field at an arbitrary point P,

$$dH = \frac{\mu o}{4*\pi} * \frac{i*dl*sin\theta}{r^2} \quad (4)$$

In equation 4, r is the distance between selected length element $\overrightarrow{dl}$ and arbitrary point P. The angle between the wire and imaginary line between $\overrightarrow{dl}$ and P is Θ.

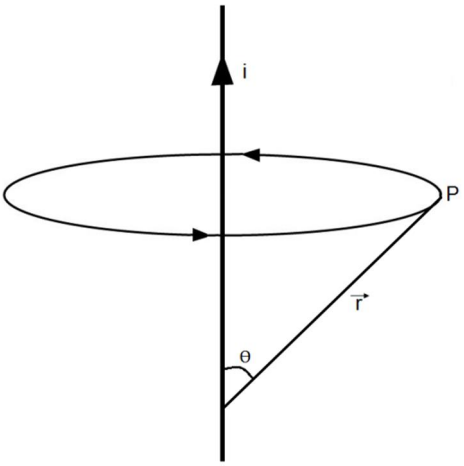

Figure 4. *Diagram of Biot-Savart law.*

The amount of magnetic flux Φ_B that penetrates an arbitrary surface area A, which is encircled by a given closed loop.

$$\Phi_B = \iint \vec{H}.d\vec{A} \quad (5)$$

The value of the amount of flux does not depend on the value of area but depends on the given loop [22].

In 1819, Oerster discovered that a steady current produces a steady magnetic field. This is a fundamental notion that connected electricity with magnetism. After that, Faraday was doing his experiment and trying to find that steady magnetic field might produce a steady current. He built up a circuit with a battery, switch, and solenoid. In general, when the switch was closed then a current was flowing that created a magnetic field in the solenoid. Faraday put a secondary loop around that solenoid. According to Faraday's thought, if there was a current flow in the circuit then the solenoid should produce a magnetic field and this magnetic field would induce current in the secondary loop but he did not find any current in the secondary loop. However, when he closed or opened that switch, he observed a current in the secondary loop.

$$\oint \vec{E}.\overrightarrow{dl} = \frac{d\Phi_B}{dt} \tag{6}$$

Therefore, he concluded few outcomes such as – the steady magnetic field never produces a steady current. The changing magnetic field causes a current in the secondary loop. Therefore, a current or electric field can be produced by the change of the magnetic field. This phenomenon is called electromagnetic induction.

2.1.2 Inductive powering for implant biotelemetry

The application of inductive power transfer system has been developed rapidly and growing its market throughout the whole world [18],[24],[25]. In the field of commercial electronics such as portable, wearable and implantable devices, this technology is becoming much more popular day by day [18],[26],[27]. In medical applications, wearable and implantable sensor devices are using wireless inductive powering [28],[29],[30],[31]. The size the receiving coil of the implanted RFID tags need to be small with respect to the transmitting coil [32]. Yates *et al.* derived a power transfer formula for a poorly coupled system where power is transferred from the transmitting coil to the receiving coil [32], [33]. When a telemetry system is involved in healthcare monitoring application, then it is denoted as the biotelemetry [34]. A biotelemetry system comprises four basic components such as sensors for a particular property monitoring, the power system of the implant device, RF antenna and receiver.

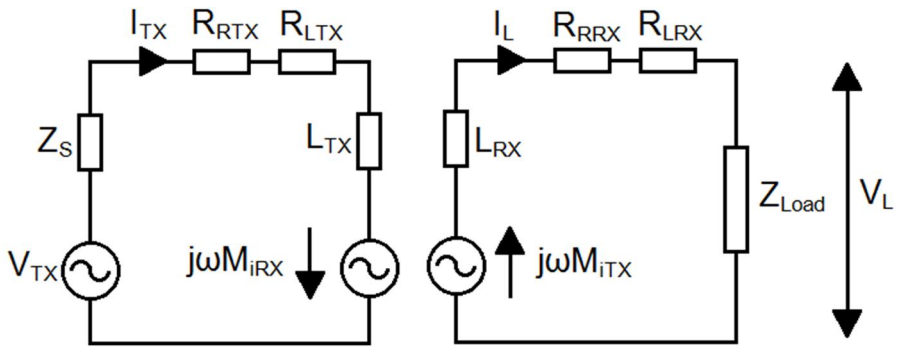

Figure 5. *Near field inductive link.*

In Figure 5, there are specific variables for the transmitter section and a receiver section. The transmitter and the receiver section are symbolized as TX and RX respectively. Z_S and Z_L are the source impedance and load impedance respectively. R_{TX} is the summation of R_{RTX} and R_{LTX}. R_{LTX} is the resistive part of inductance L_{TX}. The total resistance R_{RX} at receiver terminal is calculated like transmission terminal.

From Figure 5, on the transmitting side, Z_S needs to be resonated with L_{TX} for maximum current flow. A capacitor needs to add for resonating the inductor in the transmitter end.

$$Z_S = \frac{1}{j\omega C} \tag{7}$$

From frequency resonance equation, the value of capacitor can be calculated by,

$$C = \frac{1}{\omega^2 L_{TX}} \tag{8}$$

If a sinusoidal current $I_{TX} = I_o\, e^{j\omega t}$ starts following in transmitter for excitation where I_o is the peak current value, then the real input power can be expressed by,

$$P_{TX} = {I^2}_{TXrms}\, R_{TX} \tag{9}$$

Similarly, on the receiving end, load impedance Z_{Load} should be conjugate matched with R_{RX} for the maximum power transfer from the transmitter coil.

$$Z_{Load} = R_{RX} - j\omega L_{RX} \tag{10}$$

So, the real power at the delivery end which is transferred from transmitting antenna,

$$P_{RX} = \frac{{V^2}_{Load}}{Real\,(Z_{Load})} = \left[\frac{Z_{Load}\, Vind}{(Z_{Load} + R_{RX})}\right]^2 * \frac{1}{Real\,(Z_{Load})} = \frac{Vind^2}{4R_{RX}} \tag{11}$$

where, load voltage V_{Load} is potential divider across Z_{Load} and V_{ind} is the induced voltage [32].

From Biot-Savart law, the magnetic field at receiving antenna can be achieved with respect to transmitting antenna [32],[33],[35]. The magnetic field at receiving antenna for N turns,

$$H = \frac{I*N_{TX}}{4\pi} \oint \frac{dl \times r}{r^3} \tag{12}$$

Moreover, the induced voltage at the receiving end can be obtained by Faraday's law. This approach is valid for short range RFID tags antenna for biomedical applications [32],[36]. Usually, this approach is applicable to 1 to 5 cm apart between transmitting and receiving antenna [32],[36]. The induced voltage at receiving antenna [32] is,

$$V_{ind} = N_{RX} * \mu_o * A_{RX} * j\omega * H = \frac{N_{TX} * N_{RX} * \mu_o * A_{RX} * j\omega * I_{TXrms}}{4\pi} . H^2{}_{int} \tag{13}$$

where, $H_{int} = \int_0^{\pi} \frac{dl_{TX} \times r}{r^3}$, (14)

N_{RX} is the number of turns and A_{RX} is the area of receiver coil.

From equation 9 and equation 11, a power ratio between receiving and transmitting antenna [32] is,

$$\frac{P_{RX}}{P_{TX}} = \frac{\mu^2{}_o * N^2{}_{TX} * N^2{}_{RX} * A^2{}_{RX} * \omega^2 * H^2{}_{int}}{16 * \pi^2 * R_{TX} * R_{RX}} \tag{15}$$

2.2 Wireless link modeling

Wireless power transfer to the implant can overcome the drawback of battery dependent implant device [15]. In the near field inductive link, two antennas are used for coupling. These antennas are capable of transferring both power and data. An external antenna is placed outside of the body and the implant antenna is situated inside [15]. Wireless link modeling is a convenient way to replicate the practical scenario into the virtual vicinity. There are two subsections to articulate link modeling – two port network & simulation model.

2.2.1 Two port network

A two-port network is an electrical network with four terminals (Figure 6). These terminals are connected to external devices. This network can be described by four external variables - voltage V_1 and current I_1 at the input port, and voltage V_2 and current I_2 at the output port. A two-port network can be analyzed by few models such as impedance model, admittance model, transmission model, and hybrid model. However, here only the impedance model is discussed in detail.

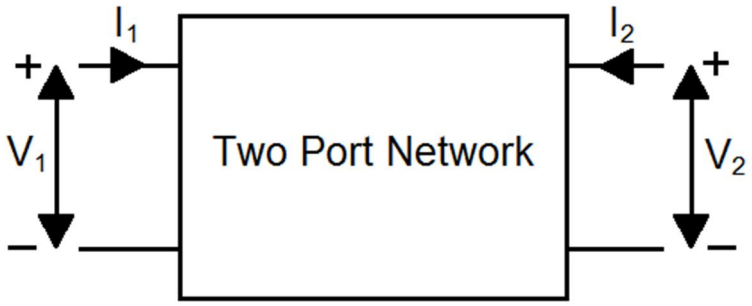

Figure 6. *Two port network.*

A near field inductive link consists of two coupled antennas. An inductive link model can be characterized by the linear microwave two-port network, consists of Z-parameters [37],[38]. All the mathematical derivations for the inductive link model are elaborately described in the simulation model section. An inductive link model is defined as a two-port network and after that, it is solved by using the impedance model.

2.2.2 Simulation model

The Simulation model of an inductive link is developed by using the principle of the two-port network [37],[39]. M. Mark *et al.* introduced the layered tissue model in their research article [15],[40]. This layered tissue model is used to mimic the notion of a wireless link through biological tissue. ANSYS HFSS ver. 2016.1 is used to develop the simulation model. The model contains four basic elements: 2 mm of skin, 2 mm of fat, 6.4 mm of cortical bone and brain (gray matter). The thickness of cortical bone has been varied with respect to different modeling performance analysis. Dielectric properties are frequency dependent and they are properly assigned. All the data of dielectric properties are taken from the research outcome of S. Gabriel *et al.* [41]. The two-port network with Z-parameters characterizes the inductive link system by the coupled antenna. This is a straightforward approach to analyzing the power transfer. By this way, transducer gain (G_P) and maximum power gain, or link power efficiency, or maximum available power gain (G_{Pmax}) can be described properly [38],[42]. G_P means the ratio between the delivered power to the sensor and available power at the external antenna terminal. Similarly, G_{Pmax} is the maximum value of G_P. In an inductive link model, the transmitting and implant antennas are conjugate matched [42].

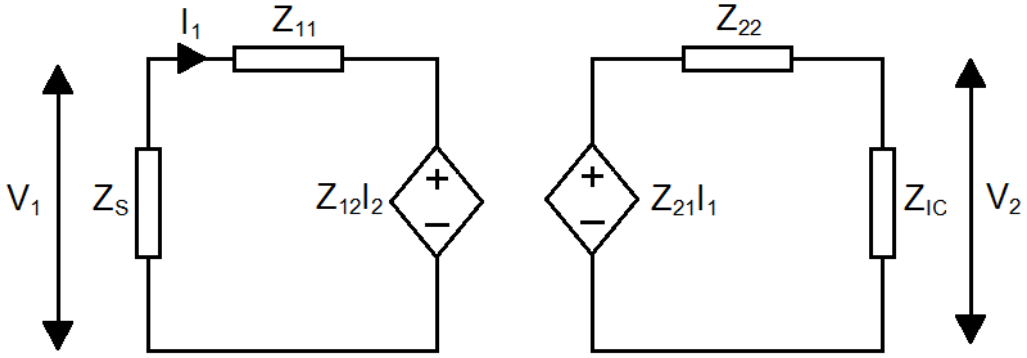

Figure 7. *Z-parameter model for near field inductive link.*

Figure 7 represents a two-port network in terms of Z-parameters, the input impedance of transmitting antenna and implant antenna are Z_{ta} and Z_{ra} [42],[44].

$$Z_{ta} = R_{ta} + jX_{ta} = Z_{11} - \frac{Z_{12}Z_{21}}{Z_{22}+Z_{IC}} \tag{16}$$

$$Z_{ra} = R_{ra} + jX_{ra} = Z_{22} - \frac{Z_{12}Z_{21}}{Z_{11}+Z_S} \tag{17}$$

Z_S and Z_{IC} are source input impedance and IC input impedance respectively. They should be defined in such a way that, they are conjugated matched to the antenna's ports [42]. RF link coupling between the transmitting antenna and the implant antenna is comparatively small ($|Z_{12}Z_{21}| \approx 0$) [42]. Therefore, based on appropriate estimation, source impedance should be conjugate matched to the transmitting antenna ($Z_S = Z_{ta}{}^*$). Correspondingly, load impedance should be conjugate matched to the receiving antenna ($Z_{IC} = Z_{ra}{}^*$) [42]. The equation of operating power gain and maximum operating power gain can be expressed in terms of two port Z-parameters [45],

$$G_p = \frac{|Z_{21}|^2}{|Z_{22}+Z_{IC}|^2}\frac{Re(Z_{IC})}{Re(Z_{11}+\frac{Z_{12}Z_{21}}{Z_{22}+Z_{IC}})} \tag{18}$$

$$G_{pmax} = \frac{|Z_{21}|^2}{S+\sqrt{S^2+|Z_{12}Z_{21}|^2}} \tag{19}$$

$$S = 2Re(Z_{11})Re(Z_{22}) - Re(Z_{12}Z_{21}) \tag{20}$$

The available power on chip IC can be defined by the operating power gain. This power is converted into DC for IC operation.

$$P_L = G_{pmax} \cdot P_{tmax} \tag{21}$$

In this equation 21, P_{tmax} is the maximum power that can be transmitted to the implant IC without violating specific abruption rate (SAR) limitations. Biological tissues can absorb electromagnetic energy when the source of this energy is exposed in front of those tissues. According to the regulations of U.S. FCC, the safety margin of SAR must be equal or

below than 1.6 W/kg. This measurement is averaged over a volume containing one gram of biological tissues [46]. On the surface, the skin tissues are relatively close to the transmitting antenna with respect to other internal tissues and skin tissues absorb the maximum electromagnetic energy as well as it has maximum SAR values. For a near field inductive link, mutual inductance becomes maximal between the transmitting and the receiving antenna depending on the ratio of the radius of the external antenna coil to the distance between antennas has a specific order of $\sqrt{2}$ [36], [42]. It can be assumed that this distance is notably larger than the radius of the implant antenna loop. However, this statement is applicable when antennas are placed in the air. Nevertheless, when the same scenario is considered including human tissues then a significant deviation can be observed. When electromagnetic energy is transmitted through the human tissues, consequently these tissues absorb a significant amount of that energy. Specific absorption rate (SAR) can be defined as the proportion of energy, which is absorbed by human tissue when tissues are exposed to an RF electromagnetic field [43]. Specific absorption rate due to electromagnetic energy can be derived from the exposed electric field to the human tissues.

$$SAR = \frac{\sigma |E|^2}{\rho} \tag{22}$$

From equation 22, it can be easily assumed that SAR is directly proportional to the exposed electromagnetic field of a specific material. Link power efficiency increases with an increase in the electromagnetic field. However, at the same time, SAR is also increasing according to the equation 22. If the value of SAR increases, the transmitted power, (P_{tmax}) becomes less. Therefore, according to the equation 22, ultimately received power at the implant device is a tradeoff between link power efficiency and SAR. A designer should consider both factors to obtain the maximum power at the implant end. Based on IEEE std C95.3-2002 in HFSS, which is an SAR calculator, a numerical modeling is obtained of the peak spatial average SAR (SAR_{max}) over one gram biological tissues [37]. Based on this phenomenon, the maximum transmitting power can be expressed as,

$$P_{tmax} = \frac{1.6W/kg \times \tau_{S-ta}}{SAR_{max}} \times P_t \tag{23}$$

Where P_t is the simulation test power and $\boldsymbol{\tau}_{S\text{-}ta}$ is the power transmission coefficient between the source and transmitting antenna. This power transmission coefficient can be expressed in terms of two port Z-parameters,

$$\boldsymbol{\tau}_{\text{S-ta}} = \frac{4Re(Z_{ta})Re(Z_S)}{|Z_{ta}+Z_S|^2} \tag{24}$$

The voltage gain of RF linked antennas and IC is the ratio of the voltage at IC end to the voltage at the transmitting antenna end. Voltage gain can be expressed in terms of two port Z-parameters [45],

$$A_V = \left| \frac{Z_{12} Z_{IC}}{Z_{11}(Z_{22}+Z_{IC}) - Z_{12} Z_{21}} \right| \quad (25)$$

From A_V, voltage at IC terminal can be determined,

$$V_L = V_{in} A_V \quad (26)$$

Where V_{in} is the voltage amplitude at the transmitting antenna in proportion to P_{tmax}. With the transmitting antenna impedance Z_{ta}, V_{in} can be expressed as [37],

$$V_{in} = \sqrt{\frac{2|Z_{ta}|^2}{Re(Z_{ta})} P_{tmax}} \quad (27)$$

Besides, the voltage amplitude at IC terminal is [37],

$$V_L = \sqrt{\frac{2|Z_{IC}|^2}{Re(Z_{IC})} \tau_{ra-IC} P_L} \quad (28)$$

where, $\tau_{ra-IC} = \frac{G_p}{G_{pmax}}$ is the power transmission coefficient and it is determined by the implanted antenna input impedance (Z_{ra}) and IC input impedance (Z_{IC}).

3. WEARABLE ANTENNA OPTIMIZATION

An external wearable antenna is used for power transfer to the implant device. It is necessary to transmit sufficient power to the implant antenna as if; an implant circuit can activate and run its operation properly. The goal of this chapter is to investigate and explore the utmost external antenna design. The existing wearable antenna model is discussed in Section 3.1. Different studied antennas are presented in Section 3.2. This section is divided into five individual subsections. Amongst the studied antennas, the best performing antenna is further optimized. The approach of antenna optimization is presented in Section 3.3.

3.1 Existing wearable antenna model

A solid two-turns circular antenna is the reference antenna which was designed by M. W. A. Khan, the doctoral student and research assistant of WISE research group [15],[16]. The antenna is presented in Figure 8. He developed this type of antenna for inductive powering to the implant [15]. The inner and outer circle diameters are 8.25 mm and 16.25 mm respectively. The width of the antenna is 8 mm and the thickness of the substrate is 1.6 mm. On both sides of the substrate, the antenna circles are exactly similar and they are connected by copper tape.

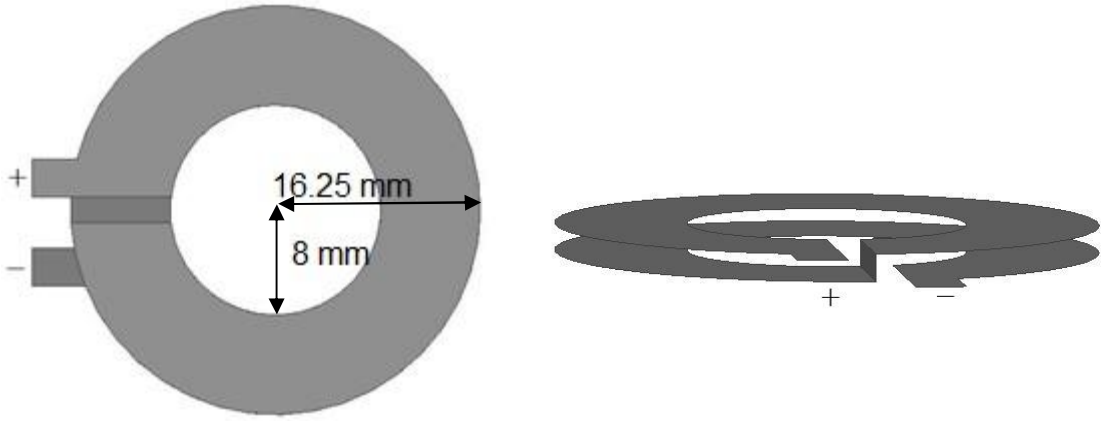

(a) *(b)*

Figure 8. *Existing two turns antenna. (a) Top view, (b) side view.*

From link model setup, it can be seen that the value of link power efficiency (G_{pmax}) is -3.34 dB. However, the exposed electromagnetic field is relatively higher and consequently the SAR value is also higher, that leads less transmitted power to the implant. The value of P_{tmax} is 974.18 mW. Therefore, the ultimately received power (P_L) at implant

is 451.97 mW or 26.55 dBm. This value of received power is taken as the reference for all the other studied antennas

3.2 Studied antenna designs

Every research has some specific reasons and objectives to overcome the existing problem or limitation. The main objective of researching on antenna design is to find an optimum external antenna. The optimized antenna should transmit maximum possible power to the implant through a tradeoff between link power efficiency and SAR. The antenna should have good link power efficiency value and low SAR. There are many existing antenna structures for example, two turns [15],[16],[38], segmented [47], and tilts [48]. In this section, five different antenna structures are studied.

3.2.1 Circular two-turns antenna with capacitor

Circular two-turns antenna with a capacitor is a modified version of existing two-turns antenna. In this model, one capacitor is used for segmenting the loop shown in Figure 9. According to M. Mark *et. al.* capacitor provides a uniform allotment of current along the loop antenna [40]. Uniform current distribution provides uniform E-field. If the E-field is uniformly distributed then the SAR impact on the tissue layer will be reduced [40]. Inspiring from these concepts, one capacitor is attached with two turns loop for segmentation. There are two individual models due to the placement of capacitor - bottom layer and top layer.

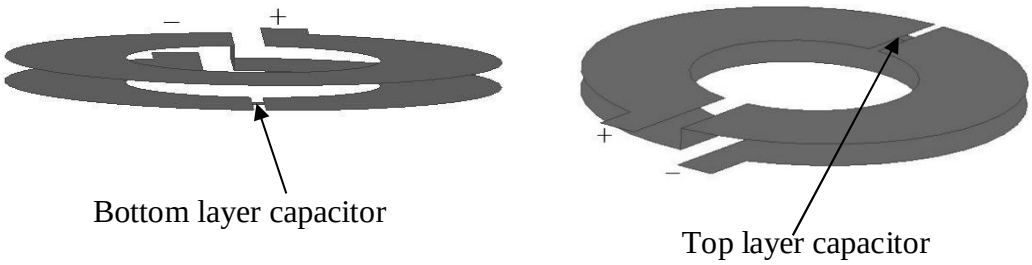

(a) *(b)*

Figure 9. *Circular two-turns antenna with capacitor. (a) Capacitor at bottom layer, (b) Capacitor at top layer.*

Structural parameters are kept as similar as the two-turns circular antenna. In addition, it is kept 5 mm apart from the skin. Results for three different capacitor values (0.6 nF, 2 nF, and 20 nF) are highlighted in Table 1 though the simulation is done from 0.1 nF to 20 nF. Transmitted power is slightly increased due to the low electric field as well as low

SAR. However, G_{pmax} decreases, therefore, overall P_L is lower for both cases compared to [15],[16],[38]. Two-turns loop antenna with the capacitor segmentation is unable to transmit higher power at the implant than solid the two-turns loop antenna.

Table 1. *Two-turns antenna with capacitor.*

Capacitor value (nF)	G_{pmax} (dB)		P_{tmax} (mW)		P_L (mW or dBm)	
	Bottom layer	Top Layer	Bottom layer	Top layer	Bottom layer	Top layer
0.6	-6.35	-6.35	1491	1499.80	345.74 or 25.39	346.17 or 25.39
2	-5.30	-5.22	1129.38	1116.09	333.38 or 25.23	335.66 or 25.26
20	-5.02	-4.73	1063.03	989.29	334.72 or 25.25	332.61 or 25.22

3.2.2 Benzene shape

The idea of benzene shape has come from the research on the segmented loop antenna [37],[47] done by E. Moradi *et al.* and T. Bjorninen *et al.* They used the capacitor for the segmentation of the antenna loop. The main purpose behind the segmentation process is to distribute E-field uniformly and by this way, the impact of SAR reduces significantly [40]. However, they used this model for 400 MHz. Benzene shaped structure concept is used in this platform where all the systems are designed for 15 MHz. Initially, for the experimental purpose a single turn benzene shape loop is taken with five segments [47] and each segment have 2 µF capacitors. The height of the antenna is 28 mm and the width of the loop is 5.2 mm. Later, the same setup is kept but the value of the capacitor is changed by 2 mF and 1 mF shown in Figure 10 below. For the setup of five segments & 2 µF, maximum transmitting power is higher than two turns loop but the link power efficiency is quite lower and the overall received power at the implant is unsatisfactory. However, 2 mF and 1 mF are not practically feasible because they have high parasitic element values and the size of the capacitor become larger. After that, another model is designed without any capacitor, which is named solid benzene loop. From the Table 2, the relation between link power efficiency and maximum transmitting power in inversely related and they change with a similar ratio.

Table 2. *Comparison between five segments and solid loop benzene shaped single turn antenna.*

Capacitor value	G_{pmax} (dB)	P_{tmax} (mW)	P_L (mW or dBm)
5 segment & 2 µF	–7.90	1535.05	249.08 or 23.96
5 segment & 2 mF	–4.19	1224.56	467.45 or 26.70
5 segment & 1 mF	–4.73	1243.83	418.63 or 26.22
Solid (no capacitor)	–5.46	1277.09	363.26 or 25.60

Another trial is taken where five segments are compressed to two segment, which is shown in Figure 10. Instead of five capacitors, one equivalent capacitor is used (see Figure 10(c)) and observed the outcomes. However, yet again there is no sign of considerable vacillation comparing with the loop of five segments, which is shown in Table 3.

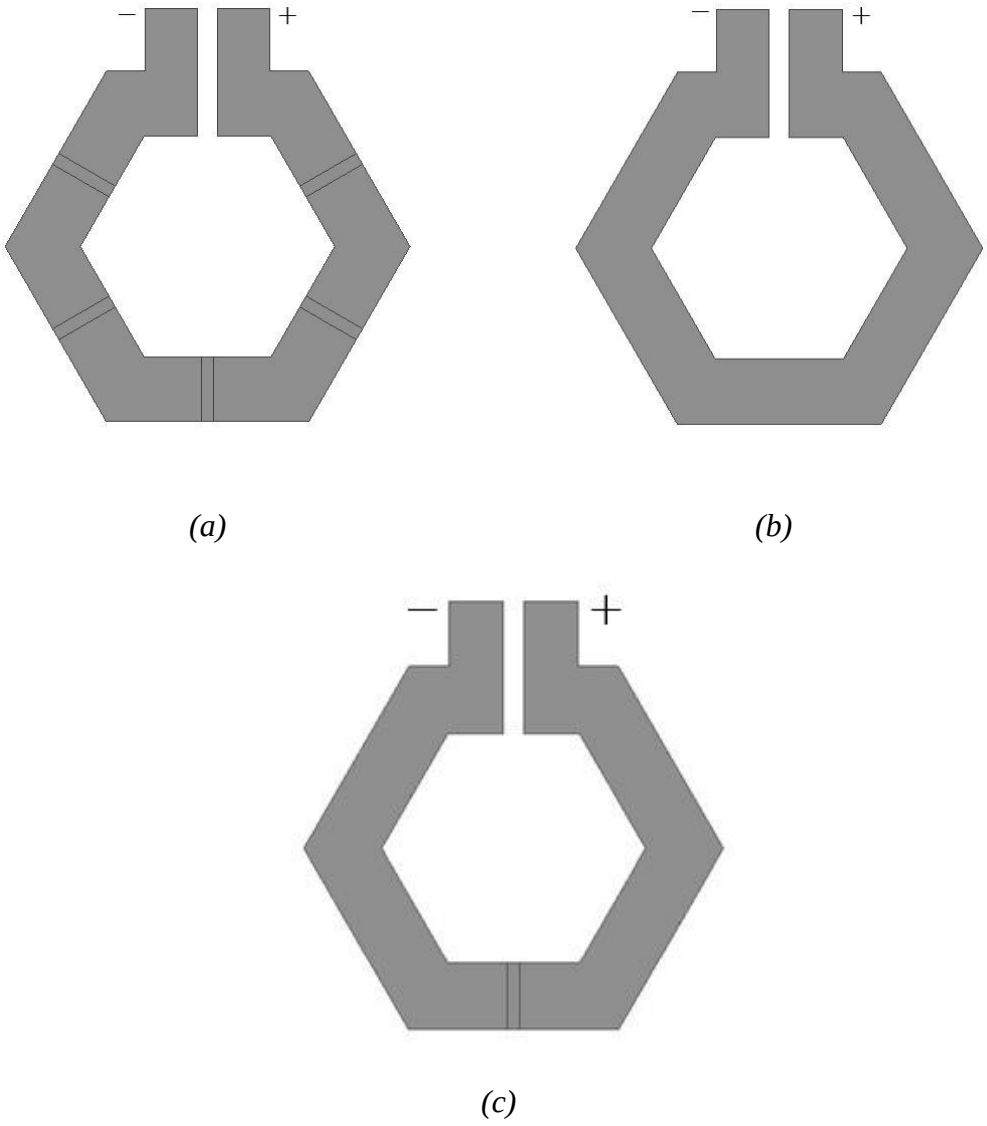

Figure 10. *Single turn benzene shape antenna. (a) Five segments, (b) Solid loop, (c) Two segment antenna.*

Table 3. *Comparison between five segments and one segment benzene shaped antenna.*

No. of Capacitor	G_{pmax} (dB)	P_{tmax} (mW)	P_L (mW or dBm)
5 Segment (2 mF each)	-5.26	1278.59	380.83 or 25.81
2 Segment (equivalent cap. 0.4 mF)	-5.45	1319.30	373.83 or 25.73
Decrease 4 Segment	3.64% decrease	3.18% increase	0.31% decrease

After getting unsatisfactory results from the trial with the one-sided loop, there is another trial taken for the two-sided antenna. For this trial, both five segments loop and solid loop structure are considered. Dimensions of structures are kept like the one-sided loop. Figure 11 is presenting two-sided antenna structure. For this trial, three separate simulations are

run for perfect observation. Outcomes of those simulations are shown in Table 4. However, these antennas are also not giving any reasonable consequence with respect to the existing two turns loop antenna.

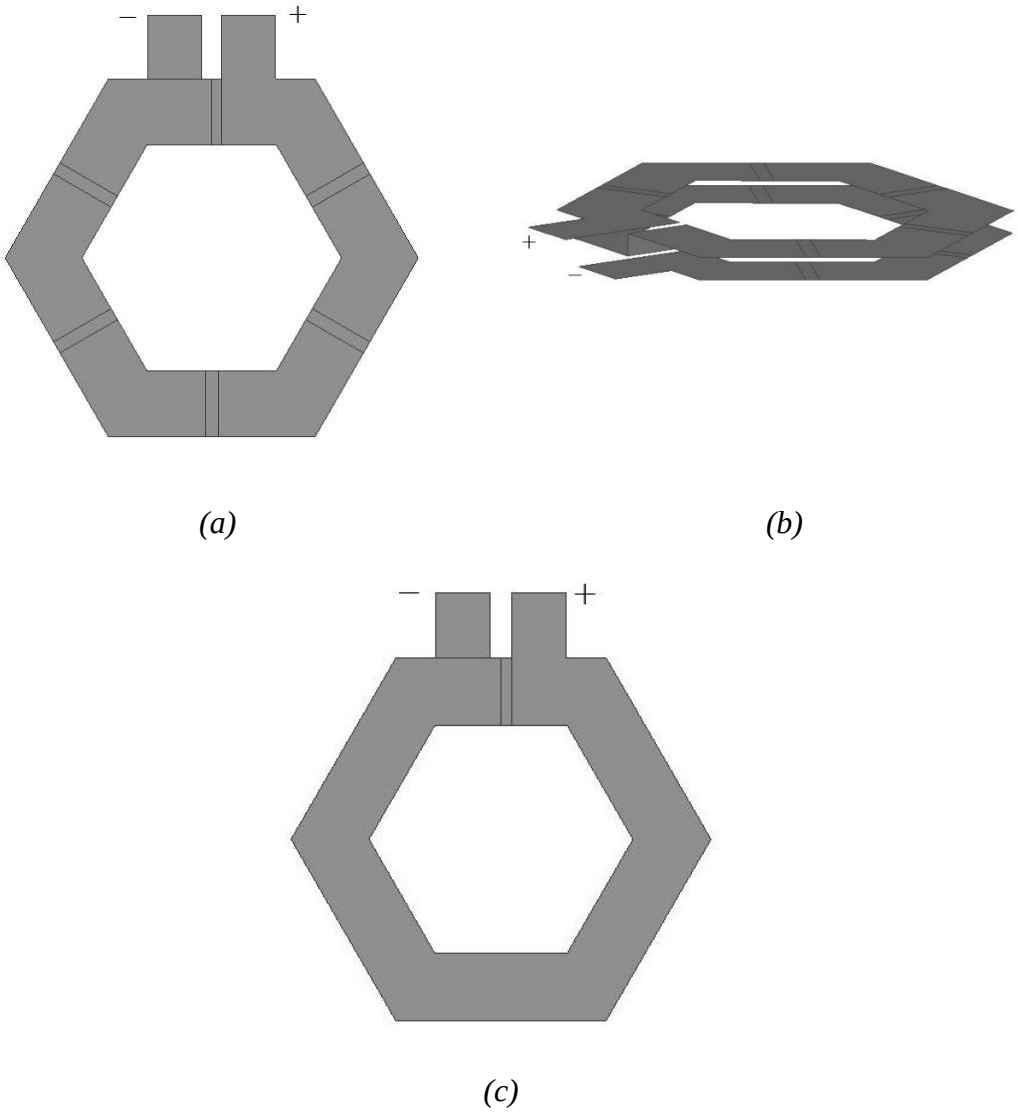

(a) *(b)*

(c)

Figure 11. *Two-turns benzene shape antenna. (a) Five segments, (b) Side view of five segments loop, (c) Solid loop.*

Table 4. *Comparison between five segments and solid loop benzene shaped two turns antenna.*

Capacitor value	G_{pmax} (dB)	P_{tmax} (mW)	P_L (mW or dBm)
5 segment & 100 µF	–4.32	1009	373.55 or 25.72
5 segment & 100 pF	–24.50	5796.28	20.57 or 13.13
Solid (no capacitor)	-4.63	951.043	327.29 or 25.15

3.2.3 Rectangular shape

Rectangular shaped antennas are based on three-dimensional structures. Antennas are mounted on the top, bottom, and edge of the substrate. For this trail, the length and height are kept equal to 34 mm and the gap between two feed points is two mm. there are two different sets of models with the different width of the antenna (7 mm and 11 mm). However, change of width is made by changing the inner rectangular area. Inner rectangular lengths are 24 mm and 16 mm for 7 mm and 11 mm respectively. Models are shown in Figure 12.

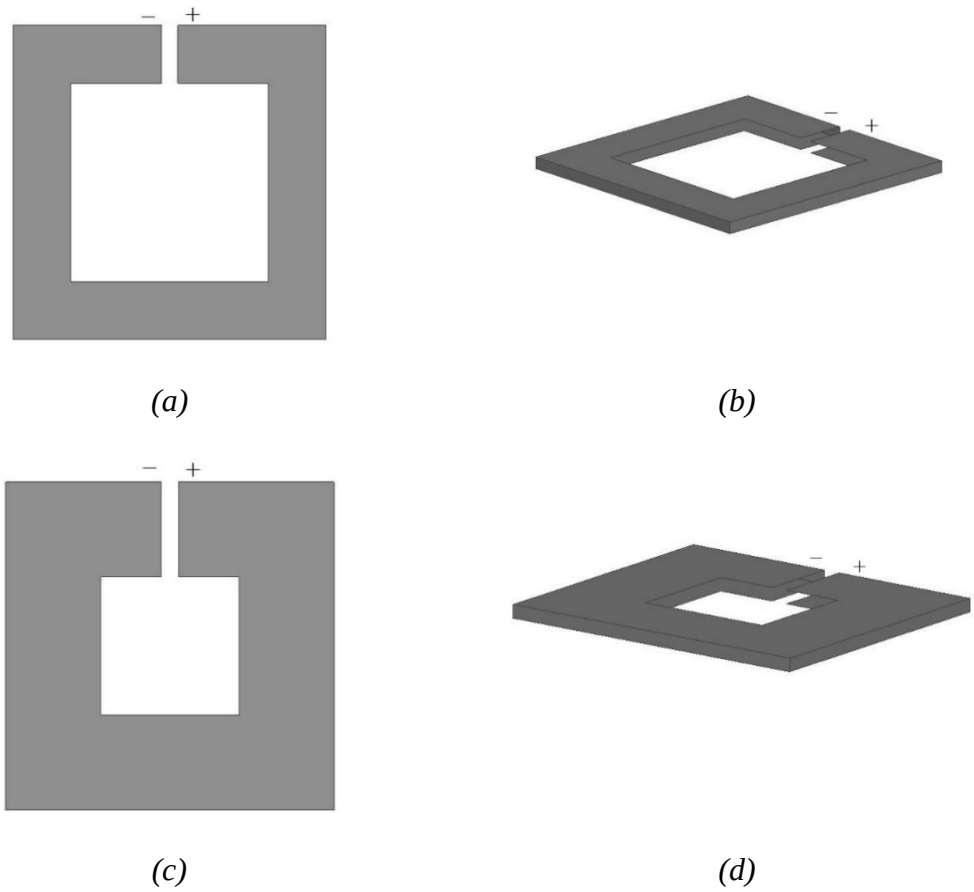

Figure 12. *Rectangular antenna structure. (a) Top view of 7 mm width antenna, (b) Side view of 7 mm width antenna, (c) Top view of 11 mm width antenna, (d) Side view of 11 mm width antenna.*

From the Table 5 both the models provide good link power efficiency although in terms of power transmission they are unable to show any prospective results. Thus, the overall received power at the implant end is lower with respect to existing two turns. The distribution of E-field is only accumulated near the feed points and there is no impact on the rest of the structure. This reason directly affects the outcomes, where satisfactory link power efficiency. Simultaneously high SAR value leads to decrease the overall transmitting power.

Table 5. *Rectangular antenna performance with the variation of antenna width.*

Width (mm)	G_{pmax} (dB)	P_{tmax} (mW)	P_L (mW or dBm)
7	-4.57	859.90	300.54 or 24.78
11	-4.98	1068.31	339.08 or 25.30

3.2.4 Octagonal spiral shape

The main idea of octagonal spiral shape comes out from benzene shaped structures. Nevertheless, in these structures, a single loop is divided into spirals. There are two trial models such as counter structure and the same directional structure. For the counter directional model, outer spacing and inner spacing are 30 mm and 10 mm respectively and for same directional structure height and inner spacing are 32 mm and 19.06 mm respectively shown in Figure 13 below. However, spacing between the spirals and thickness of spirals play a vital rule on the value of electric and magnetic field. For primary observations, both spacing and thickness are kept 0.93 mm.

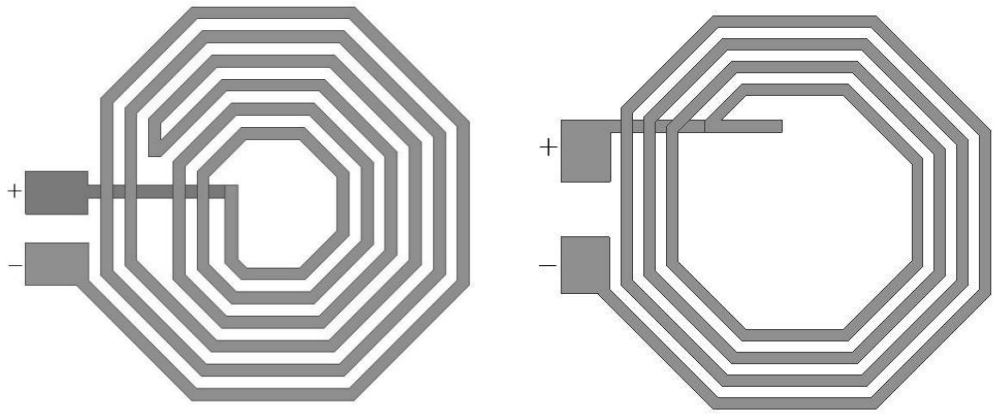

(a) *(b)*

Figure 13. *Octagonal antenna structure. (a) Top view of the counter directional loop, (b) Top view of the same directional loop.*

According to Ampere's law, when a current is passing through a wire then this current produces an electromagnetic field surrounding it. The direction of the field is defined by right-hand rules. When, a current is flowing through a same directional loop then all the fields for overall loop are accumulated. For this reason, link power efficiency becomes higher. However, for counter directional structures, electromagnetic fields are opposing with one loop to another and the overall electromagnetic field decreases. After simulation, the same theoretical phenomenon is proved, which is shown in Table 6. For the same direction, link power efficiency is satisfactory whereas the counter directional loop provides the worst results. In addition, according to previous discussions, transmitted power

is directly related with the electromagnetic field. In this case, transmitted power for the same direction is quite low while the counter direction affords a very high level of power transmission. Nevertheless, in both cases, they are not able to reach the margin of existing antenna performance.

Table 6. *Octagonal antenna performance with the change of loop direction.*

Direction	G_{pmax} (dB)	P_{tmax} (mW)	P_L (mW or dBm)
Same direction	-4.85	1030.82	337.85 or 25.29
Counter direction	-11.86	5736.10	373.83 or 25.73

3.2.5 Circular spiral shape

Circular spiral shape notion comes out from the octagonal spiral antennas but in a circular shape. In these structures also, a single loop is divided into spirals. Similar the octagonal shape, there are also two trial models such as counter structure and same directional structure. For the counter directional model, the outer and inner diameter are 32 mm and 12 mm respectively and for same directional structure, outer and inner diameter are 32 mm and 18 mm respectively shown in Figure 14. However, in terms of spacing between the spirals and thickness of spirals, there is some variation for better observations. Counter-directional structure has 2 mm spacing and thickness whereas same directional structure has 1 mm shown in Figure 14. Same directional structure is a one-sided loop but the counter directional antenna has spirals on the both side.

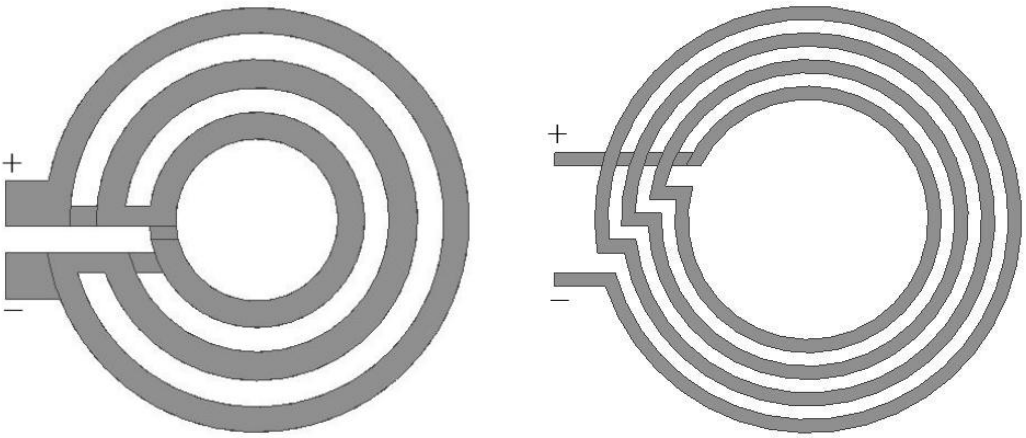

(a) *(b)*

Figure 14. *Circular spiral antenna structure. (a) Top view of the counter directional loop, (b) Top view of the same directional loop.*

Similar to octagonal spiral shape, circular spiral antennas are also following Ampere's law. A similar pattern of performance is observed between octagonal and circular shape although circular counter directional structure has very high-transmitted power shown in Table 7 and high receiving power at the implant end. This creates further attention for analysis.

Table 7. *Circular spiral antenna performance with the change of loop direction.*

Direction	G_{pmax} (dB)	P_{tmax} (mW)	P_L (mW or dBm)
Same direction	-5.54	1208.66	337.20 or 25.28
Counter direction	-11.12	6313.75	488 or 26.88

Now modification is done for improving the antenna structure. In this case, both same and counter directions are merged into one structure. It is a simple one-sided loop structure and four spirals where three spirals are in one direction but one spiral is in the different direction (Figure 15). Initially, the spacing and thickness of spirals are kept 1 mm each. To compare with two turns antenna, the inner and outer circle diameter are kept identical to 8.25 mm and 16.25 mm respectively (Figure 15).

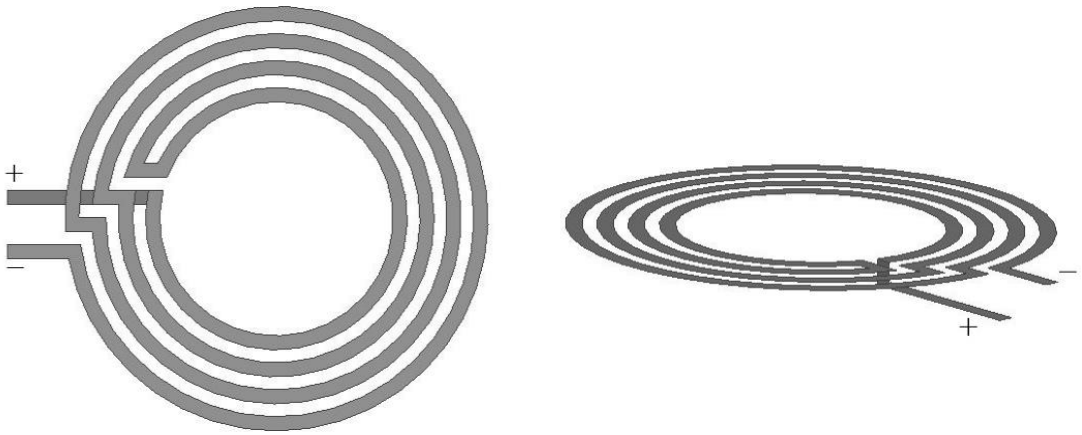

(a) *(b)*

Figure 15. *Circular spiral antenna structure with 3 turns same directional and 1 turn counter direction. (a) Top view, (b) Side view.*

If all the spirals are arranged in the same direction, then the electromagnetic field will be higher but at the same time, SAR will also be higher. Again, if two spirals are in an identical direction and other two spirals are in different, and then the generated electromagnetic field will be resisted by one another. For this reason, the overall electromagnetic field will be lower and concurrently SAR will also be lower.

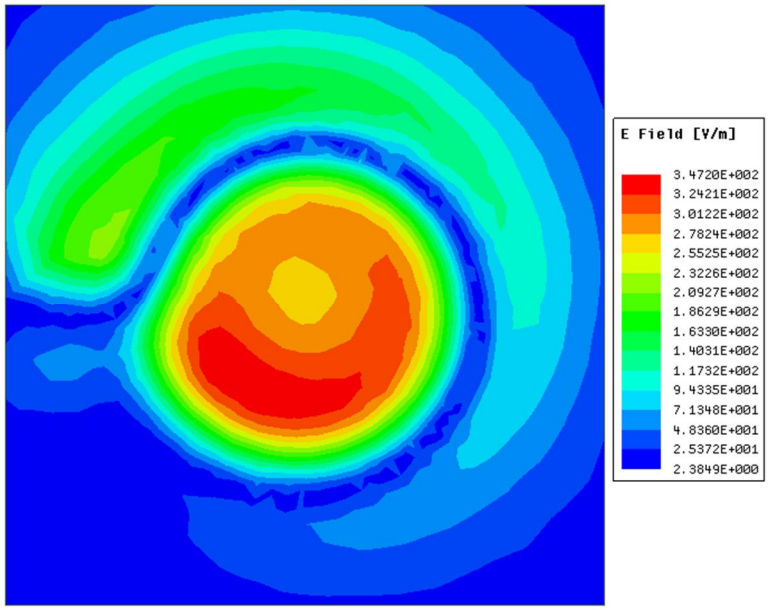

Figure 16. *E-field distribution of circular spiral antenna structure with 3 turns same directional and 1 turn counter direction.*

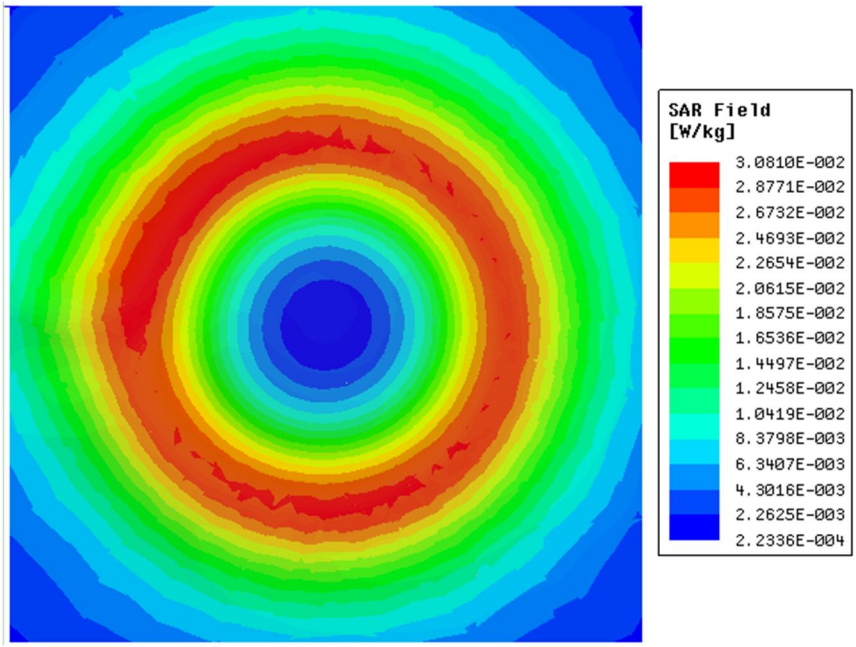

Figure 17. *Local SAR distribution of circular spiral antenna structure with 3 turns same directional and 1 turn counter direction.*

From Figure 16 and Figure 17, perhaps local SAR, which is generated by the circular spiral antenna, is uniformly distributed. Moreover, there are two uneven peaks of E-field. One robust peak of E-field is generated in the inner diameter and there is another long but trivial peak, which is observed at the outside of the spiral loop. To achieve a remarkable

received power at the implant, link power efficiency and SAR will be tradeoff by modifying antenna structure. In this case, three spirals are in an identical direction but one spiral is in the dissimilar path. From Table 8 it can be seen that this model works where link power efficiency is still lower but acceptable and all together transmitted power is much higher of 2610.44 mW. Therefore, this model provides 603.02 mW or 27.80 dBm to the implant, which is almost 25% higher than existing two turns antenna model.

Table 8. *Comparison between existing two turns antenna and circular spiral (3 turns same directional and 1 turn counter direction).*

Antenna type	G_{pmax} (dB)	P_{tmax} (mW)	P_L (mW or dBm)
Two-turns model	-3.34	974.18	451.97 or 26.55
Circular spiral	-6.37	2610.44	603.02 or 27.80

Circular spiral antenna creates a space for further improvement and several steps are used for optimization. The approach of antenna optimization is briefly discussed in the next section.

3.3 Optimized spiral antenna: Behavior of spacing and thickness variation

After the observation of five different antennas performance, it is found that; the circular spiral antenna executes improved results than the existing antenna model. The circular spiral antenna provides 25% more power for the implant device although it has 3 dB less link power efficiency than the existing model. The main goal of this section is to improve the performance of the circular spiral antenna. In Section 3.2.4, it is discussed that spacing between the spirals and thickness of spirals play a vital rule on the electric field. Although, in Section 3.2.5, the circular spiral antenna was designed with equal spacing and thickness. However, in this section, spacing between the spirals and thickness of spirals is changed to get an optimized spiral antenna. This experiment contains a range of measurement lengthwise from 0.7 mm to 1.5 mm with 0.1 mm interval both for thickness and for spacing. There are total 81 combinations of thickness and spacing and each combination represents an individual antenna structure. These combinations are used in the link model and in the SAR model. The value of link power efficiency, (G_{pmax}) and maximum transmitted power (P_{tmax}) are arranged in Table 9 and Table 10 respectively. In addition, received power (P_L) at the implant end is calculated from link power efficiency and maximum transmitted power, which is obtained in Table 11.

Table 9. *Value of G_{pmax} from link model.*

	Thickness (p)									
		0.7	0.8	0.9	1.0	1.1	1.2	1.3	1.4	1.5
Space (q)	0.7	-7.51	-7.13	-6.83	-6.61	**-6.34**	-6.10	-5.99	-5.87	-5.67
	0.8	-7.37	-7.04	-6.69	-6.40	-6.22	-5.97	-5.86	-5.74	-5.55
	0.9	-7.19	-6.89	-6.53	**-6.31**	-6.12	-5.89	-5.72	5.55	-5.40
	1.0	-7.12	-6.76	-6.50	-6.25	-6.02	-5.80	-5.62	-5.48	-5.36
	1.1	-6.98	-6.64	**-6.37**	-6.12	-5.90	-5.68	-5.51	-5.41	-5.25
	1.2	-6.87	-6.53	-6.21	-6.00	-5.76	-5.63	-5.49	-5.30	-5.18
	1.3	-6.77	-6.43	-6.15	-5.95	-5.72	-5.53	**-5.38**	**-5.25**	**-5.13**
	1.4	-6.72	-6.42	-6.14	-5.90	-5.65	-5.51	**-5.32**	**-5.19**	**-5.04**
	1.5	-6.70	**-6.29**	-6.04	-5.86	-5.63	-5.45	**-5.29**	**-5.12**	**-5.05**

Table 10. *Value of P_{pmax} from SAR model.*

	Thickness (p)									
		0.7	0.8	0.9	1.0	1.1	1.2	1.3	1.4	1.5
Space (q)	0.7	4493.44	3991.79	3519.87	3282.46	**2922.56**	2730.74	2591.67	2418.86	2349.94
	0.8	4357.65	3835.21	3386.82	3044.50	2802.66	2618.41	2444.55	2275.75	2132.90
	0.9	4018.31	3481.04	3137.48	**2872.42**	2747.34	2532.94	2354.67	2207.50	1994.81
	1.0	3850.92	3484.71	3031.55	2813.06	2559.78	2424.09	2181.02	2090.05	1912.07
	1.1	3856.57	3242.06	**2940.80**	2679.25	2521.81	2290.19	2119.52	2050.73	1900.62
	1.2	3679.59	3153.45	2856.62	2577.08	2350.42	2210.15	2088.43	1943.87	1870.85
	1.3	3490.74	3081.62	2685.70	2468.95	2325.98	2053.69	**1990.07**	**1896.30**	**1730.82**
	1.4	3323.92	2941.83	2608.87	2403.56	2226.48	2020.92	**1918.09**	**1807.25**	**1740.94**
	1.5	3326.85	**2913.65**	2608.08	2329.11	2201.60	2016.77	**1899.46**	**1777.37**	**1713.45**

Table 11. *Received power (P_L) assessment from G_{pmax} (Table 9) and P_{tmax} (Table 10).*

	Thickness (p)									
		0.7	0.8	0.9	1.0	1.1	1.2	1.3	1.4	1.5
Space (q)	0.7	797.22	772.96	729.94	716.59	**679.00**	670.24	652.57	625.78	637.33
	0.8	799.65	758.03	725.72	696.96	668.67	662.75	634.77	606.62	594.75
	0.9	767.70	723.65	698.03	**671.64**	671.56	652.18	631.38	614.57	574.73
	1.0	747.47	735.56	678.71	667.22	639.56	637.04	597.86	591.19	556.37
	1.1	773.06	702.98	**679.09**	655.06	648.22	619.83	596.08	590.73	566.91
	1.2	756.69	700.82	683.47	646.86	623.77	604.55	589.44	573.11	568.01
	1.3	735.07	700.95	651.13	626.69	623.38	574.93	**576.91**	**566.75**	**531.09**
	1.4	707.52	671.36	634.71	618.52	605.95	568.17	**563.62**	**547.07**	**545.25**
	1.5	711.19	**685.45**	649.07	604.01	602.91	574.56	**562.34**	**546.47**	**535.79**

From above tables, there are many apposite combinations and many prospective conclusions may come out. However, antenna combination can be selected depending on the appropriate applications. For the near field, wireless power transmission to implant should have a tradeoff between good link power efficiency and less SAR values. From above tables, the range of thickness and spacing of 1.3 mm to 1.5 mm, the value of P_L decreases with the increase of thickness and spacing. Although 1.3 mm and 1.3 mm has decent G_{pmax} (-5.38 dB) but among these ranges, this point provides the highest power at implant. This is the reason for primarily selecting this point. However, there is another remarkable diagonal series of values in the table of G_{pmax}. Primarily, four consecutive values of G_{pmax} are selected such as, -6.34 dB, -6.31 dB, -6.37 dB, and -6.29 dB. Each value is around 3 dB less than the existing two turns antenna (-3.3 dB).

Table 12. *Prospective antenna structure combinations.*

Antenna structure combination			G_{pmax} (dB)	P_{tmax} (mW)	P_L (mW)
Set of combinations	**Thickness (mm)**	**Spacing (mm)**			
A	1.1	0.7	-6.34	2922.56	679.00
B	1	0.9	-6.31	2872.42	671.64
C	0.9	1	-6.37	2940.80	679.09
D	0.8	1.5	-6.29	2913.65	685.45

From the Table 12, there are four sets of antenna structure available and it can be seen that the values of G_{pmax} are around -6.3 dB. Deviation of P_L of set 'A', 'C', and 'D' with respect to set 'B' are 7.36 mW, 7.45 mW, and 13.81 mW. However, there is no significant variation of power at the implant (P_L). Although for these minor deviations, 50.14 mW, 68.38 mW, and 41.23 mW more power need to transmit from the external antenna while G_{pmax} is almost alike. So, it is decided to use set 'B' whereas the level of performance is nearly similar with low power transmission.

4. PERFORMANCE COMPARISON BETWEEN TWO-TURNS AND SPIRAL CIRCULAR ANTENNA

The implanted device for intracranial pressure (ICP) monitoring is battery-free electronics based system. Power is sent to the implant device wirelessly, through inductive coupling. Transmitted power should be high enough to activate the electronics of the implant. In the previous chapter, two external antennas are primarily selected after the antenna optimization stage. However, both the antennas are assumed better but in this chapter, the best-performed antenna is characterized by standard performance analysis studies. All the studies are done in the simulation stage by ANSYS HFSS 2016.1. This chapter is designed into three sections – study of implant depth in Section 4.1, the study of skull thickness variation in Section 4.2, and study of external antenna distance from the skin surface in Section 4.3.

4.1 Study of implant depth

Inductive coupling between the external and implant antenna is the wireless powering process for a battery-free implant device. The implant device is placed inside the body tissues. External antennas should transmit power for the activation of the implant circuit. The foremost objective of this section is to develop a systematic assessment of how deep an implant can be activated by inductive powering. This demonstration is focused on measuring the intracranial pressure from the cranial subarachnoid space. A simple channel model contains 2 mm of skin, 2 mm of fat and 6.4 mm of bone tissue [50]. According to H. A. M. Mahinda *et al.* average bone tissue thickness may vary between 6.3 mm to 7 mm [49],[50]. However, for this analysis, 6.4 mm of bone tissue is considered (see in Figure 18). Grey matter of brain area is situated after the bone tissue layer. In previous studies, an implant was placed in the grey matter section of the brain after the bone tissues. Nevertheless, an external antenna with better performance compared with the existing antennas, can improve the depth and thus an implant can place further deeper.

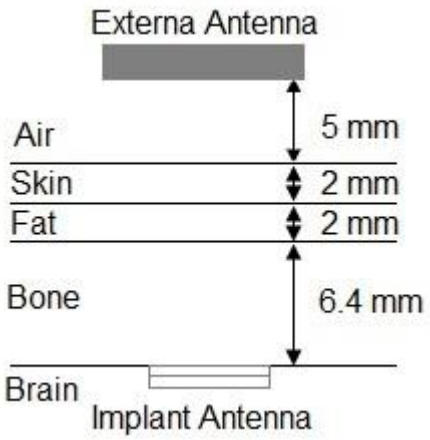

Figure 18. *Simple channel model.*

From the above Figure 18, the external antenna is placed 5 mm apart from the skin and there is another considerable part for implant coating. Implant coating has 1 mm thickness and the implant antenna including electronics is placed in the middle of coating thickness [16]. For this demonstration, 15.9 mm is the minimum inductive link distance to transmit the power from the external antenna. Inductive link distance (d_{im}) is the summation of implant depth and the external antenna distance from the skin. The minimum value of the dim is 15.9 mm, which is the summation of 5 mm air, 2 mm of skin, 2 mm of fat, 6.4 mm of bone, and 0.5 mm of the coating. The value of minimum implant depth is 10.9 mm. In this study, the depth of implant is increased, thus the implant depth as well as the inductive link distance increases.

Table 13. *Comparison between two antennas structures by changing the implant depth.*

Implant depth (mm)	Inductive link distance, d_{im} (mm)	Set X (1.3 mm & 1.3 mm)			Set Y (1 mm & 0.9 mm)		
		G_{pmax} (dB)	P_{tmax} (mW)	P_L (mW)	G_{pmax} (dB)	P_{tmax} (mW)	P_L (mW)
11	16	-5.35	1990.07	580.73	-6.22	2872.42	685.86
11.5	16.5	-5.67	1990.07	539.94	-6.63	2872.42	624.78
12	17	-5.93	1990.07	508.88	-6.92	2872.42	584.32
12.5	17.5	-6.12	1990.07	486.21	-7.19	2872.42	549.02
13	18	-6.40	1990.07	455.53	-7.55	2872.42	504.52
13.5	18.5	-6.68	1990.07	427.77	-7.80	2872.42	476.71
14	19	-6.94	1990.07	402.66	-8.12	2872.42	442.79
14.5	19.5	-7.19	1990.07	379.75	-8.44	2872.42	411.37

In this study, two different sets of circular spiral antennas (1.3 mm & 1.3 mm and 1 mm & 0.9 mm) are used for simulation. The external antenna sets are categorized based on spiral thickness and spacing between two adjacent spirals. Table 13 represents two sets of circular spiral antennas; those are assigned as "*Set X*" and "*Set Y*" respectively. From

the earlier calculations, 15.9 mm is the minimum distance to transmit power according to the channel model and now the implant depth is considered between 16 mm to 19.5 mm for both antennas. In Table 13, received power at the implant end is calculated for implant depth between 16 mm to 19.5 mm with 0.5 mm interval. From previous studies with two-turns external antenna, it can transmit around 452 mW for maximum 16 mm distance [15]. From the above Table 13, it can be observed that "*Set X*" can transmit more power than the two-turns antenna at 18 mm implant depth and after 18 mm if the implant depth is further increased then received power is lower than existing two turns antenna. Therefore, it signifies that the external antenna of "*Set X*" can transmit almost similar or more power as two-turns with 2 mm more implant depth. However, "*Set Y*" of the external antenna appears more promising from the Table 13. It can transmit 476.71 mW to the implant with total implant depth 18.5 mm. It already covers 2.5 mm more distance and still sends 24.75 mW more power than the two-turns antenna at 18.5 mm. Therefore, we have finalized the design of external antenna with thickness (1 mm) and spacing (0.9 mm) for fabrication.

4.2 Study of skull thickness variation

A human skull is a skeletal composition that contains neurocranium [51] and viscerocranium [52]. Neurocranium is known as braincase that protects the brain and brainstem [51]. Similarly, viscerocranium is known as a facial skeleton that holds major sensory organs e.g. eyes, ears, nose. [52]. The human skull is not a piece of bone but a combination of different bone regions with natural or biological sutures. In the human skull, the shape of bone, thickness and other properties are not alike for all different bone regions. However, by assuming from previous studies or experiments, intracranial pressure (ICP) can be measured from parietal or occipital bone region that shown in Figure 19.

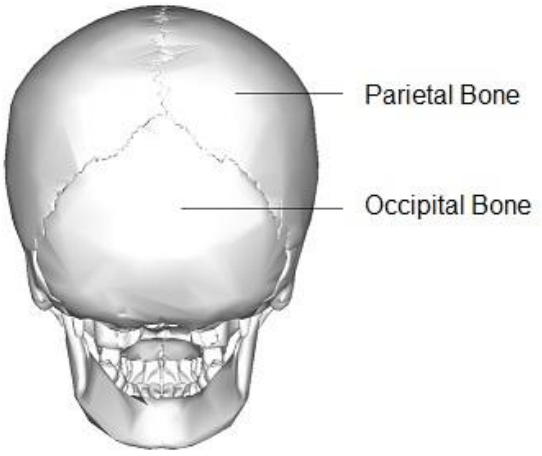

Figure 19. *Posterior of human skull.*

For an adult human, the thickness of parietal and occipital bone is also varied for male and female. According to H. A. M. Mahinda *et al.*, there is a slight difference in thickness of parietal, occipital and central occipital bones [50]. Thickness variations for male and female and for different regions are accumulated in Table 14.

Table 14. *Skull bone thickness for male and female [50].*

Bone categories	Male	Female
Parietal bone	7.7 mm	7.1 mm
Occipital bone	5.8 mm	5.6 mm
Central occipital bone	9.4 mm	8.2 mm

Therefore, the thickness variation is in between 5.6 mm to 9.4 mm. For this demonstration, the range of skull thickness is considered between 4.5 mm to 10 mm for covering the completely available range of thickness. In this demonstration, two sets of the spiral circular antenna (*Set X* and *Set Y*) are used for simulation, like Section 4.1, with the variation of skull thickness. For this study, the implant is attached to the interior side of the skull and the position of the implant is fixed in the grey matter of the brain although the thickness of the skull is changing.

As like Section 4.1, a simple channel model contains 2 mm of skin, 2 mm of fat and a range between 4.5 mm to 10 mm of bone tissue [50]. Similarly, the external antenna is placed 5 mm apart from the skin and implant antenna including electronics is placed in the middle of coating thickness. For this demonstration, 9.5 mm is the fixed distance to transmit the power from the external antenna. The minimum link distance of 15.9 mm is the summation of 5 mm air, 2 mm of skin, 2 mm of fat, 0.5 mm of the coating, and skull thickness.

Table 15. *Performance comparison between two antenna structures with the variation in skull thickness.*

Skull thickness (mm)	Inductive coupling distance, d_{im} (mm)	Set X (1.3 mm & 1.3 mm)			Set Y (1 mm & 0.9 mm)		
		G_{pmax} (dB)	P_{tmax} (mW)	P_L (mW)	G_{pmax} (dB)	P_{tmax} (mW)	P_L (mW)
4.5	14	-4.50	1990.07	706.57	-5.19	2872.42	869.18
5	14.5	-4.75	1990.07	667.06	-5.50	2872.42	809.69
5.5	15	-4.94	1990.07	638.69	-5.82	2872.42	751.55
6	15.5	-5.14	1990.07	609.73	-5.99	2872.42	723.75
6.4	15.9	-5.35	1990.07	580.31	-6.29	2872.42	675.29
6.5	16	-5.36	1990.07	579.20	-6.38	2872.42	661.33
7	16.5	-5.65	1990.07	541.92	-6.68	2872.42	616.98
7.5	17	-5.87	1990.07	515.14	-6.81	2872.42	599.17
8	17.5	-6.14	1990.07	484.07	-7.30	2872.42	534.88
8.5	18	-6.40	1990.07	455.85	-7.55	2872.42	504.54
9	18.5	-6.67	1990.07	428.92	-7.78	2872.42	478.55
9.5	19	-6.96	1990.07	401.22	-8.18	2872.42	437
10	19.5	-7.19	1990.07	380.29	-8.51	2872.42	404.63

From the Table 15, the length of skull thickness is added in 15.9 mm, where 9.5 mm is the fixed distance due to air, skin, fat and coating layer. For this study, the thickness of the skull is considered between 4.5 mm to 10 mm for both antenna sets. This range of skull thickness provides an array of inductive link distance between 14 mm to 19.5 mm. 0.5 mm is the interval between two consecutive readings for both the range of skull thickness and inductive link distance.

From the above Table 15, it can be seen that the external antenna of "*Set X*" is capable of transmitting 579.20 mW power to the implant device, which is 22% higher than the two-turns antenna. Again, the antenna structure of "*Set Y*" can transmit 661.33 mW power to the implant device. It is 31% higher with respect to the two-turns antenna. "*Set Y*" is superior to other antenna structure. This comparison is based on 16 mm inductive coupling distance and 6.5 mm skull thickness.

From the above Table 15, it can be seen that "*Set X*" can transmit more power than the two-turns antenna at 18 mm inductive coupling distance where skull thickness is 8.5 mm. However, if the skull thickness is further increased then received power is lower than the existing antenna. The external antenna of "*Set Y*" appears more satisfactory from the Table 15. It can transmit 478.55 mW to the implant with 18.5 mm inductive link distance where skull thickness is 9 mm. Therefore, the external antenna of "*Set Y*" can cover up to 9 mm of skull thickness, which is 2.7 mm higher than the average skull thickness.

4.3 Study of external antenna distance and implant depth from the skin

The placement variation of antenna influences the performance of power transmission to implant. Wireless power is transmitted through few specific layers such as – air, skin, fat, skull and brain. These layers have their own properties and cross-sectional thickness is one of the major criteria among them. The thickness variation of layers may directly affect the overall system. This study is designed to observe the performance and received power at the implant device for the variation of external antenna distance and implant depth with respect to the skin. According to Section 4.1 and 4.2, the external antenna of "*Set Y*" has proved for its better performance. For this reason, this demonstration is done by the circular spiral antenna with thickness (1 mm) and spacing (0.9 mm).

Table 16. *G_{pmax} combinations and P_{tmax} for circular spiral antenna with thickness (1 mm) and spacing (0.9 mm).*

G_{pmax} combination (dB)			Distance between external antenna and skin (mm)				
			5	4	3	2	1
	Implant depth (mm)	11	-6.36	-5.72	-5.29	-4.71	-4.30
		12	-6.83	-6.20	-5.80	-5.39	-4.77
		13	-7.46	-6.80	-6.25	-5.73	-5.38
		14	-8.23	-7.23	-6.77	-6.35	-5.70
		15	-8.62	-8.13	-7.46	-6.95	-6.29
P_{tmax} (mW)			2610.43	2018.23	1641.01	1178.13	921.28

From Table 16, there are five different distances of the external antenna with respect to the skin and five consecutive implant depths from the skin. Link power efficiency is calculated by the combination of external antenna distance and implant depth with the help of the link model. There are 25 of link power efficiency combinations in total. For example, by keeping external antenna distance 5 mm with respect to skin, implant depth is increasing from 11 mm to 15 mm with 1 mm interval.

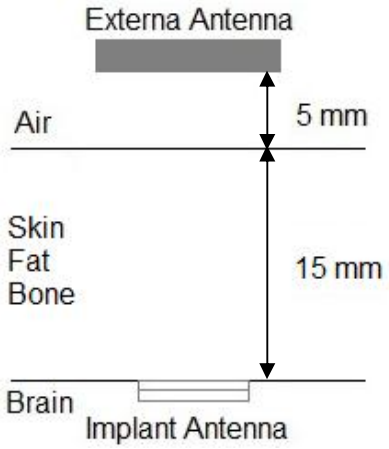

Figure 20. *Channel model demonstration for 5 mm distance of external antenna and 15 mm implant depth.*

Figure 20 shows the channel model demonstration for 5 mm distance of external antenna and 15 mm implant depth. The similar phenomenon is followed for 4 mm, 3 mm, 2 mm and 1 mm. Again, in SAR model, P_{tmax} is calculated for different distance between the external antenna and skin. P_{tmax} is not affected by the change of implant depth. It only depends on the distance between the external antenna and skin. P_{tmax} is decreased if the distance between external antenna and skin is reduced. However, for a particular distance between the external antenna and skin if the implant depth is increased, then link power efficiency is decreased.

Table 17. *Output power at implant device, which is calculated from Table 16.*

P_L (mW)		Distance between external antenna and skin (mm)				
		5	4	3	2	1
Implant depth (mm)	11	603.02	540.21	485.72	398.37	342.13
	12	541.69	484.03	432.14	340.36	307.11
	13	468.50	422.04	389.01	315.20	267.20
	14	392.13	381.54	345.18	272.83	248.02
	15	358.64	310.66	294.34	238.45	216.73

Table 17 accumulates all the received power at the implant end. These data are calculated from the link power efficiencies combinations and maximum transmitted power from Table 16. From Table 17**,** it can be seen that the external antenna can efficiently work if the distance between the external antenna and skin is within 5 mm to 3 mm. For 5 mm distance, there are three efficient reading for 11 mm, 12 mm and 13 mm implant depth. Again, for 4 mm distance, there are two efficient reading for 11 mm, and 12 mm implant depth. In addition, for 3 mm distance, there is only one efficient received power at 11 mm implant depth. These received powers at the implant are compared with the previous antenna's performance (452 mW). From Table 17, it can be concluded that, if the distance of the external antenna is reducing then the possibility of getting efficient power at the implant is decreased with the degradation of maximum transmitted power, although, link power efficiency looks satisfactory. When the external antenna is brought closer to the skin then, the SAR increases and as a result, P_{tmax} decreases rapidly. Although there is an increment in G_{pmax} with small distance but the impact on SAR is greater compared with G_{pmax}.

5. EXPERIMENTAL SETUP AND MEASUREMENT

This chapter provides an experimental based statement about the applicability of optimally designed wearable antenna in a realistic phase. In Chapter 4, several studies are executed for the performance analysis between the spiral circular antenna and two-turns antenna in simulation stage. Based on those performances analysis, it is decided to fabricate the spiral circular antenna for further experiments in the biological environment. This chapter contains two individual sections. In Section 5.1, the process of antenna fabrication and the matching circuit are described briefly. In addition, in Section 5.2, the fabricated antenna is tested in two ways – "*air gap testing*" and "*air and pigskin gap testing*". Section 5.3 provides an assessment of performance comparison between "*in vitro*" experiments.

5.1 Antenna fabrication and matching circuit

Antenna fabrication and adding the matching circuit with the fabricated antenna are two separate steps. Antenna fabrication processes are done in the etching laboratory. In the electronics lab, matching circuit elements are affixed with that fabricated antenna.

5.1.1 Antenna fabrication

The process of antenna fabrication is completed in the etching laboratory. Initially, the final artwork or antenna model is prepared in ANSYS HFSS 2016.1 with proper dimensions. Substrate area layout of 41 mm × 41 mm is also included with the antenna model. Antenna model has two layer – top and bottom layer, which is shown in Figure 21.

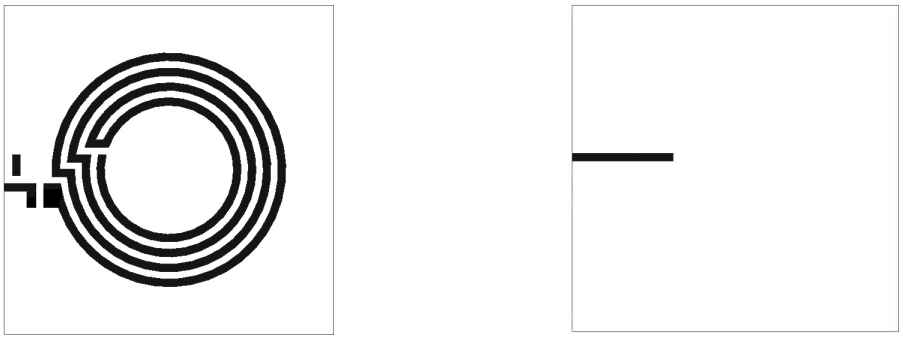

(a) *(b)*

Figure 21. *Layout of antenna, which is printed for fabrication process. (a) Top layer, (b) Bottom layer.*

Subsequently, the top and bottom layer are separately printed on two different transparent papers, which is called film. Two identical transparencies are exactly fixed by tape on each other to make a two-sided film. There are three basic steps in the etching laboratory such as – substrate dimension fixation by cutting step, ultra-violate (UV) exposure, and chemical processing (Figure 22).

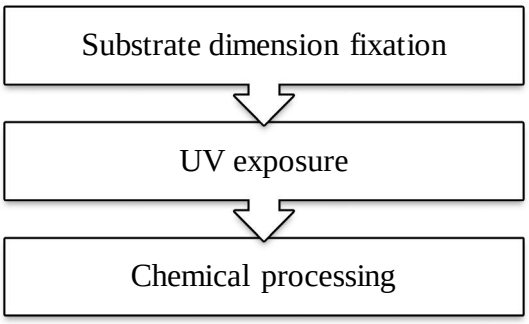

Figure 22. *Basic work flow diagram for fabrication process.*

A double-layer printed circuit board (PCB) covering blue film with the dimensions of 41 mm × 41 mm is used for antenna fabrication. Ultra-Violate (UV) exposing machine is used for 40 seconds to print the layout on the substrate. After UV exposure, that substrate is assigned for further chemical processing. Antenna fabrication should be very precise. If there is any discontinuity in the loops/spirals, then the new antenna must be fabricated because discontinuities deteriorate the overall performance of the antenna.

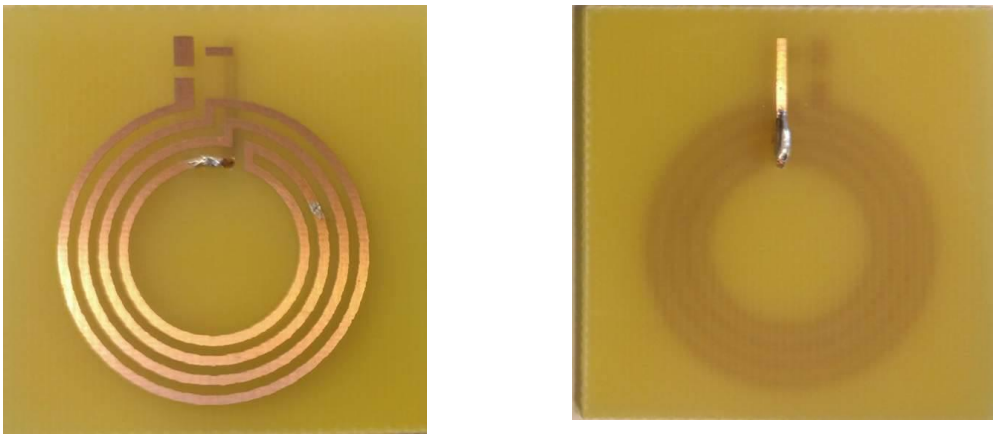

(a) *(b)*

Figure 23. *Fabricated circular antenna. (a) Upper layer, (b) Bottom layer.*

Figure 23 shows the fabricated circular spiral antenna. This substrate has both sided copper layer. The upper layer is connected with the bottom layer by copper tape. A small hole is created by the drill machine and soldered a copper tape with the main structure of the antenna.

5.1.2 Matching circuit

Maximum power transfer from the source to load is ensured when the impedance properly matched between transmitting and receiving terminals. The matching circuit is used for impedance matching. For an RF circuit, the impedance should be matched in such a way that, the real part of source needs to be equal to the real part of the load. Moreover, for the reactance, source reactance should be equal to load reactance but in opposite character. Impedance matching is usually done with the combination of capacitor and inductor or single capacitor. The components value and the pattern of the matching circuit are determined from Z-parameters at the operating frequency. A LC impedance matching network designer [53] is used for determining L and C values. The value of capacitance and inductance are 318.5 pF and 50.44 nH. However, these values are not directly available in the laboratory. Instead of 318.5 pF and 50.44 nH, the closest values of 324 pF and 47 nH are used respectively.

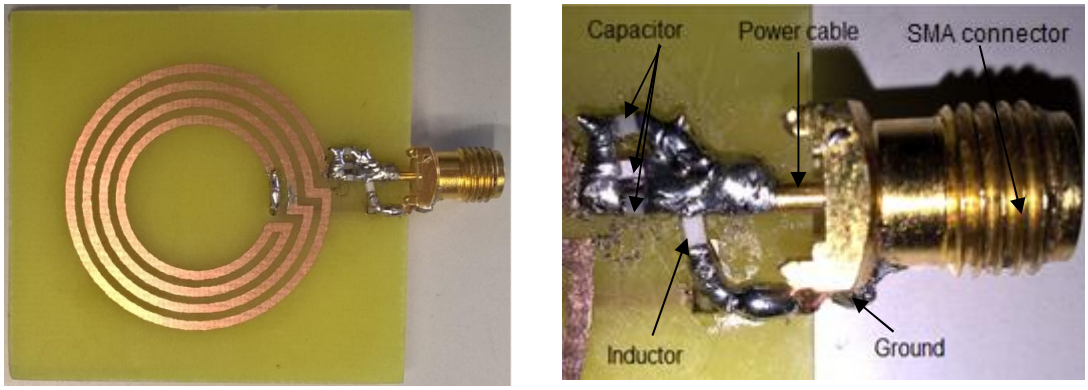

(a) *(b)*

Figure 24. *Practical matching circuit, connected with circular spiral antenna. (a) Top view overview of antenna including matching circuit and SMA connector, (b) Close view of matching circuit.*

Figure 24(a) provides a complete illustration of the antenna including matching circuit and Figure 24(b) focuses on the matching circuit and sub-miniature version A (SMA) connector. An inductor of 47nH and capacitor of 324 pF are connected in parallel in an LC matching configuration. A cable connector is added for the convenient use and it is quite easy to connect with other cables by using sub-miniature version A (SMA) connector.

5.2 Performance analysis of circular spiral antenna

After the finalization of the process of fabrication and accumulation of the matching circuit, circular antenna passes through a couple of "*in vitro*" test. Testing procedures are categorized into two sections – testing with the air gap, and testing with the air-pig skin

layer. Both testing procedures are elucidated based on S-parameter analysis. Vector network analyzer (VNA) in the laboratory measures S-parameters. The vector network analyzer (VNA) has two ports – port 1 and port 2. Both ports of VNA are calibrated before the beginning of S-parameters measurement. However, data from VNA is saved in '. s2p' file format for each distance. According to the S-parameter measurement equations of two-port network, S_{11} and S_{22} belong to the external antenna and implant antenna parameter respectively. Similarly, S_{12} and S_{21} are the forward gain or insertion loss and reverse gain or insertion loss respectively. S_{12} and S_{21} both are identical. A pre-built implant circuit is used in port 2, which was developed by M. W. A. Khan [15],[16],[38].

5.2.1 Air gap testing

Air gap testing evaluates the performance of power transmission from the external antenna to the implant circuit. In the air gap testing method, a minimal weight, white thin-layered Styrofoam is used as separation between the external and implant antenna. The external antenna is connected with port 1 and implant antenna is connected to port 2 of VNA. This test procedure is performed with four different coupling distances – 14 mm, 16 mm, 18 mm, and 20 mm. Available Styrofoam has two different thicknesses – 2 mm and 4 mm. Coupling distances are arranged with the combination of available Styrofoam. Styrofoam is properly marked to place the antenna accurately to avoid the misalignment between antennas. In Figure 25 shows the both top and side view of properly positioned antennas with apposite separation.

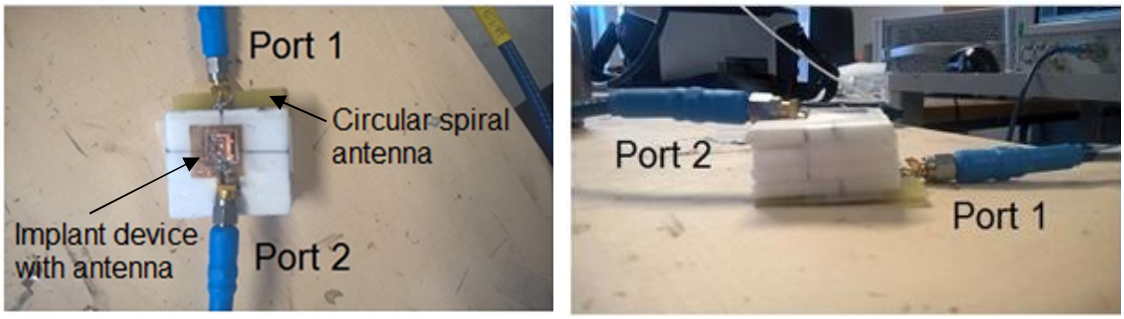

(a) *(b)*

Figure 25. *Experimental setup for air gap testing. (a) Top view, (b) Side view.*

Reading of S-parameters is recorded for each consecutive distance (14mm, 16 mm, 18 mm, and 20 mm). Output Data of S-parameter from VNA is saved in '. s2p' file format for each distance. However, a similar setup is simulated in the software for making the comparison between simulated data and measured data. In the Table 18, first three columns are presenting S_{11}, S_{22}, and S_{12} for both simulation and measurement.

Table 18. *Performance analysis of coupling between antennas with air gap testing.*

Distance (mm)	S_{11} (dB)		S_{22} (dB)		S_{12} (dB)		G_{pmax} (dB)		
	Simulation	Measurement	Simulation	Measurement	Simulation	Measurement	Simulation (with parasitic)	Simulation (without parasitic)	Measurement
14	-5.07	-6.97	-4.89	-5.52	10.73	-10.88	-6.86	-4.89	-8.66
16	-5.90	-7.33	-3.99	-4.73	-12.28	-12.74	-8.36	-5.96	-10.27
18	-5.80	-7.46	-3.48	-4.44	-13.90	-14.23	-9.68	-7.08	-11.65
20	-6.36	-7.28	-3.08	-4.00	-15.57	-16.03	-11.27	-8.33	-12.78

For simulations, '. s2p' files are assigned in the n-port of circuit design section of the software and for measurement, '. s2p' files are imported to the analysis section. A visual representation can be obtained of S-parameters in graphical format. A visual illustration for simulation and measurement are separately presented in Figure 26 and Figure 27.

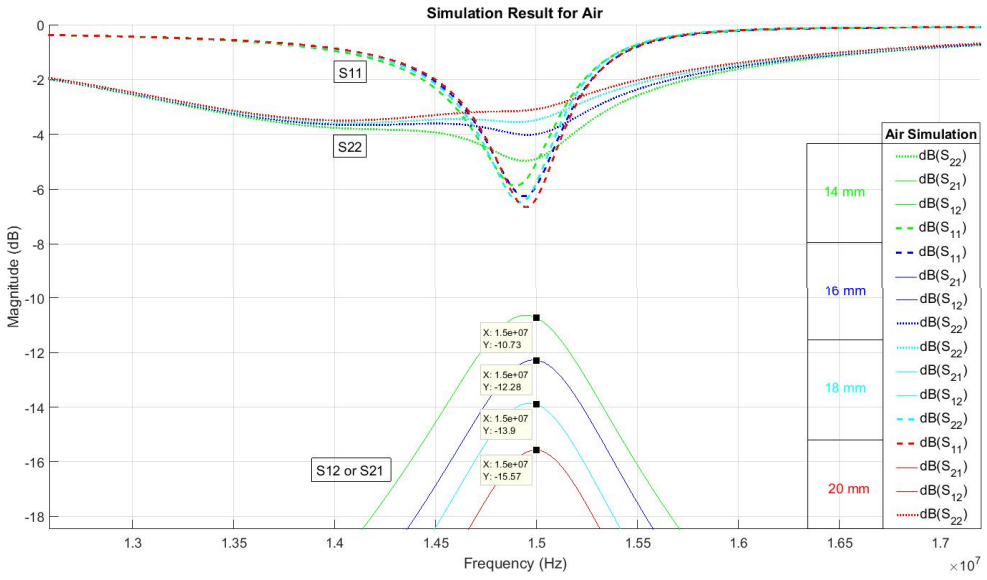

Figure 26. *S-parameters for the simulation of air gap testing.*

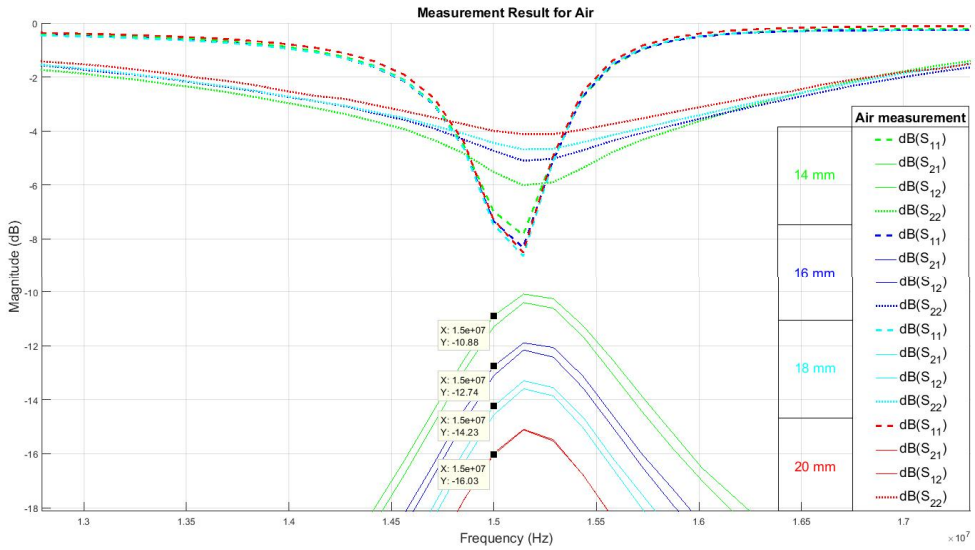

Figure 27. *S-parameters, measured by VNA in air gap testing.*

From Table 18, it can be also shown that S-parameters for simulations and measurements for different distances are relatively comparable and meaningful. S-parameters are decreasing with the increase of distances. On the same table, G_{pmax} is categorized into three sections. Measured G_{pmax} can be obtained from measured S-parameters. Moreover, G_{pmax} is also found in simulations. There are two kinds of simulations – matching circuit design with parasitic values and without parasitic values. The difference between parasitic values and without parasitic values shows the loss due to the matching circuit.

5.2.2 Air and pigskin testing

The air gap including pigskin testing is another way to evaluate the performance of power transmission from the external antenna to the implant circuit. In this method, a 6-mm wide pigskin layer is used, which is shown in Figure 28.

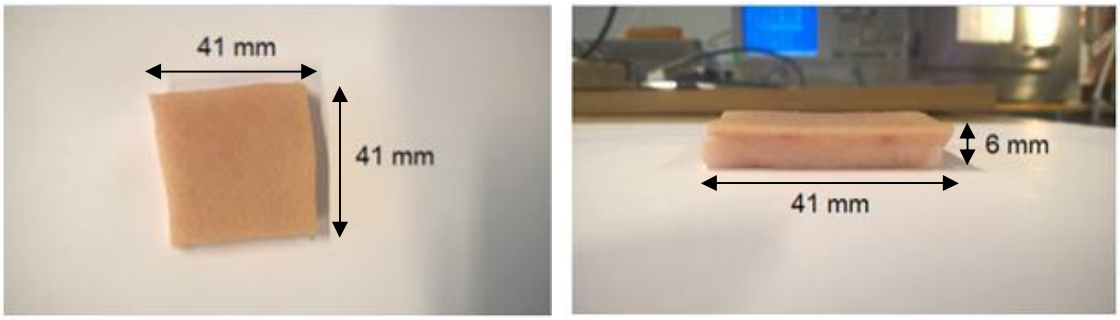

(a) *(b)*

Figure 28. *Dimension of pigskin layer. (a)Top view, (b) Side view.*

A Pigskin layer with 6 mm thickness contains 2 mm of skin and 4 mm of fat (Figure 28). This processed pigskin layer is prepared into 41 mm × 41 mm size. Like air gap testing, this test procedure is also performed with four different coupling distances – 14 mm, 16 mm, 18 mm, and 20 mm (Figure 29). These distances are built up by a 6-mm pigskin layer and layered Styrofoam. The external antenna is connected with port 1 and implant antenna is connected to port two of VNA. Antennas are properly positioned to avoid the misalignment between antennas. Figure 29 shows the both top and side view of properly positioned antennas with apposite separation.

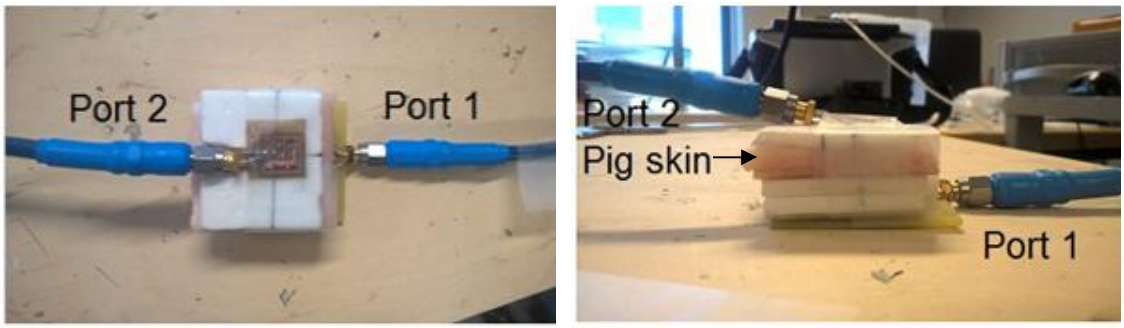

(a) *(b)*

Figure 29. *Experimental setup for pigskin and air gap testing. (a) Top view, (b) Side view.*

Similar to air gap measurement, the reading of S-parameters is recorded for each consecutive distance (14mm, 16 mm, 18 mm, and 20 mm) and the output data of S-parameter from VNA is saved in '. s2p' file format for each distance. In the Table 19, again first three columns present S_{11}, S_{22}, and S_{12} for both simulation and measurement.

Table 19. *Performance analysis of coupling between antennas with pigskin and air gap testing.*

Distance (mm)	S_{11} (dB)		S_{22} (dB)		S_{12} (dB)		G_{pmax} (dB)		
	Simulation	Measurement	Simulation	Measurement	Simulation	Measurement	Simulation (with parasitic)	Simulation (without parasitic)	Measurement
14	-4.54	-6.99	-4.96	-5.45	-10.75	-11.50	-6.75	-4.86	-9.17
16	-5.78	-7.17	-3.95	-4.80	-12.31	-13.35	-8.31	-5.94	-10.76
18	-5.79	-7.26	-3.58	-4.50	-13.98	-14.77	-9.85	-7.26	-12.20
20	-5.66	-7.38	-3.19	-4.16	-15.65	-16.82	-11.22	-8.46	-14.00

Generated '. s2p' files from simulations and measurement by VNA for each individual distance are used for further analysis and graphical representations. Again, for simulations, '. s2p' files are assigned in the n-port of circuit design section of the software and for measurement, '. s2p' files are imported to the analysis section. A visual representation can be obtained of S-parameters in graphical format. A visual illustration for simulation and measurement are separately presented in Figure 30 and Figure 31.

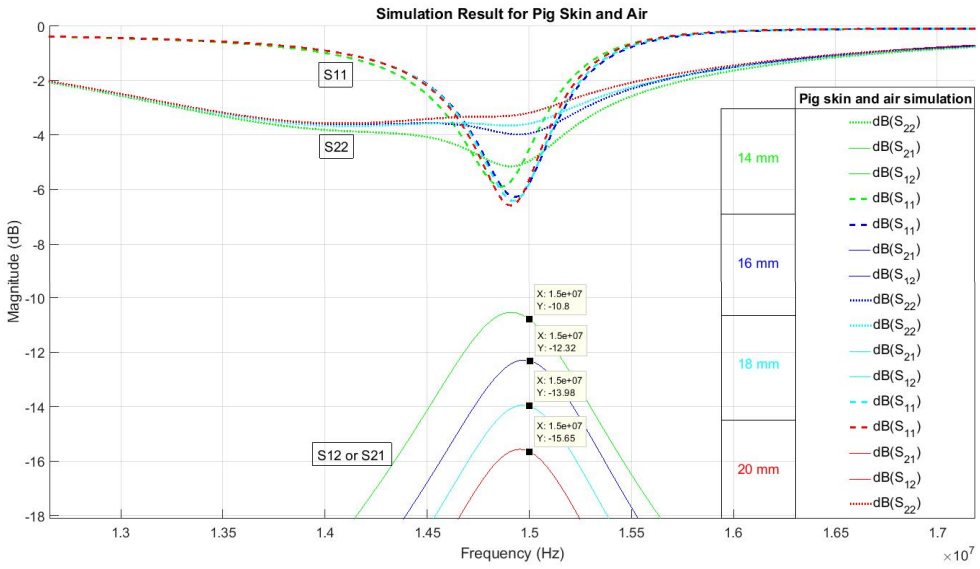

Figure 30. *S-parameters for the simulation of pigskin and air gap testing.*

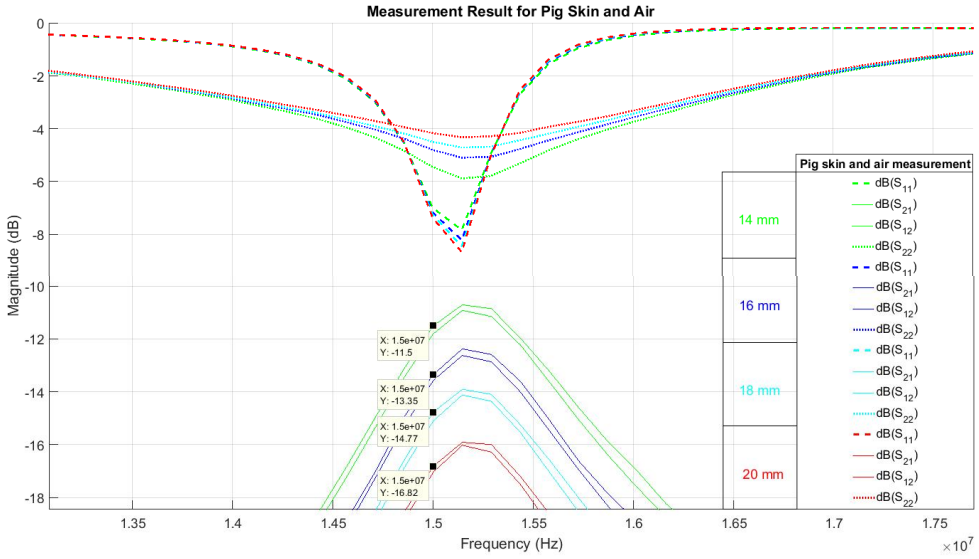

Figure 31. *S-parameters, which is measured by VNA in pigskin and air gap testing.*

From Table 19, it can be also shown that the values of S-parameters are decreasing with the increase of distances. On the same table, there are three individual G_{pmax} is categorized – measured G_{pmax}, simulated G_{pmax} with the matching circuit excluding parasitic elements, and simulated G_{pmax} with the matching circuit including parasitic elements.

5.3 Performance comparison

Performance comparison section combines both air gap testing and air gap with pigskin testing. These analytical statistics are drawing out from Table 18 and Table 19 effect of parasitic elements and pigskin impact are discussed briefly.

5.3.1 Impact of parasitic elements

Earlier in Section 5.1.2, it is discussed that, in practical use, an inductor has some capacitors in parallel and resistor in series as a parasitic element. Similarly, when a capacitor is used, it has some parasitic elements such as inductor and resistance in series. These additional parasitic elements consume a certain amount of power. Before the experiment, it was assumed that the difference due to parasitic elements should be an identical digit for both the experiment of “Air gap testing” and “Air gap and pig skin testing”. In addition, after the experiment, the assumption is verified and the difference due to the parasitic element is almost identical. Table 20 represents the difference of G_{pmax} due to parasitic elements for both the experiments.

Table 20. *Variation of link power efficiency (G_{pmax}) and the impact of parasitic elements for different link distances.*

Distance (mm)	Air gap testing			Air gap and pig skin testing		
	Without parasitic (dB)	With parasitic (dB)	Difference (dB)	Without parasitic (dB)	With parasitic (dB)	Difference (dB)
14	-4.89	-6.86	1.97	-4.86	-6.75	1.89
16	-5.96	-8.36	2.40	-5.94	-8.31	2.37
18	-7.08	-9.68	2.60	-7.26	-9.85	2.59
20	-8.33	-11.27	2.94	-8.46	-11.22	2.76

5.3.2 Measured S12 parameter

Pigskin of 6 mm thickness contains 2 mm of skin and 4 mm of fat. Pigskin is a biological object and it should have higher dielectric properties and it should absorb more transmitting power due to skin and fat layers. However, Table 21 shows the effect of pigskin presence on *S12*.

Table 21. *Impact on S_{12} due to pigskin for different coupling distances.*

Distance (mm)	Air medium (dB)	Air and pig skin medium (dB)	Difference (dB)
14	-10.88	-11.50	0.62
16	-12.74	-13.35	0.61
18	-14.23	-14.77	0.54
20	-16.03	-16.82	0.79

From Table 21, it can be seen that, the value of S12 decreases with an increase in the distance between external antenna and implant antenna. The similar scenario happens for both “Air medium” and “Air and pig skin medium”. Although the coupling distance is increased but the same pigskin layer is used for each measurement. According to the previous postulation, due to the introducing of the pigskin layer, the value of “Air and pig skin medium” should be constantly lower than “Air medium” with a particular difference and this difference indicates the impact of the pigskin layer. However, on the right most column of the Table 21, it shows that the difference is almost identical value although the coupling distance is increased. This analysis supports the assumed postulate.

6. CONCLUSION

The concept of wireless power transfer by inductive coupling can be used for the power transmission of the medical implant devices. The target is to develop a wearable and external antenna for transferring sufficient power to the implant for its activation. The aim is to ensure the maximum power transmission to the implant without violating the regulations of specific absorption rate limits. The goal of this research is successfully achieved. Concurrently with the antenna design, the simulation tools are used for creating a virtual environment of biological structure. The measurement setup is also developed for analyzing the performance of the designed antenna.

The circular spiral antenna is developed as an external antenna for transferring power to the implant device. This antenna is designed for 15 MHz frequency. It is capable of providing 25% more power at the implant end with respect to previously developed two-turns antenna. For 16 mm link distance, the circular spiral antenna provides 686 mW power for the implant. When the implant depth increases, the power transmission capability becomes decrease because of the increment of link distance. Previously developed two-turns antenna could transmit 452 mW for 16 mm link distance, which is taken as the reference result. The circular spiral antenna can transmit the same level of power of the two-turns antenna (452 mW) with the link distance of 18.5 mm. If the circular spiral antenna is used for power transmission, then the implant can be placed 2.5 mm further deeper comparing with the two-turns antenna. From skull thickness study, the circular spiral antenna can transmit the similar power of the two-turns antenna for 9 mm thick skull, whereas 6.4 mm is the average skull thickness.

Two experimental setups are developed for antenna performance analysis. In the experiment measurement, the effect of parasitic elements over the link power efficiency is identical to both the experiments. The impact on S-parameter due to a 6-mm pigskin layer is also identical to different link distances. The value of link power efficiency and S-parameter are evenly decreased with an increase in link distance, which is perfectly supporting the simulations.

From the performance analysis, in both the virtual environment and experimental setup, the circular spiral antenna has enough potentiality to use in inductive powering for further research and development. The plan of the newly developed antenna is with implement for intracranial pressure (ICP) monitoring. Finally, the spiral circular antenna can be used for versatile medical applications for wireless power transmission to the implant.

REFERENCES

[1] B. Mokri, “The Monro-Kellie hypothesis: Applications in CSF volume depletion,” *Neurology*, vol. 56, no. 12, pp. 1746–1748, 2001.

[2] T. Partington and A. Farmery, “Intracranial pressure and cerebral blood flow,” *Anaesth Intens Care*, vol. 15, pp. 189–194, 2014.

[3] S. A. Mayer, Ji Y. Chong, “Critical care management of increased intracranial pressure,” *J. Intensive Care Med.*, vol. 17, no. 2, pp. 55–67, Mar. 2002.

[4] M. Smith, “Monitoring intracranial pressure in traumatic brain injury,” *Anesth. Analg.*, vol. 106, no. 1, pp. 240–248, Jan. 2008.

[5] L. Rangel-Castillo, S. Gopinath, C. S. Robertson, “Management of intracranial hypertension,” *Neurol. Clin.*, vol. 26, no. 2, pp. 521–541, May 2008.

[6] Ghajar J, “Traumatic brain injury”, *Lancet. 356 (9233): 923–9. doi:10.1016/S0140-6736(00)02689-1. PMID 11036909, September 2000.*

[7] R. Beer, P. Lackner, B. Pfaust, E. Schutzhard, “Nosocomial ventriculitis and meningitis in neurocritical care patients,” *J. Neurol.*, vol. 255, no. 11, pp. 1617–1624, Nov. 2008.

[8] P. H. Raboel, J. Bartek Jr., M. Andresen, B. M. Bellander, B. Romner, “Intracranial pressure monitoring: invasive versus non-invasive methods – a review,” Crit. Care Res. Pract., vol. 2012, article ID: 950393, Mar. 2012.

[9] A. Aschoff, P. Kremer, B. Hashemi, S. Kunze, “The scientific history of hydrocephalus and its treatment,” *Neurosurg. Rev.*, vol. 22, pp. 67–93, Oct. 1999.

[10] F. M. Kashif, G. C. Verghese, V. Novak, M. Czosnyka, T. Heldt. “Model-based noninvasive estimation of intracranial pressure from cerebral blood flow velocity and arterial pressure,” *Sci. Transl. Med.*, vol. 4, no. 129, pp. #–#, Apr. 2012.

[11] U. Kawoos, M.-R. Tofighi, R. Warty, F. A. Kralick, A. Rosen, “In-vitro and in-vivo trans-scalp evaluation of an intracranial pressure implant at 2.4 GHz,” *IEEE Trans. Microw. Theory Techn.*, nol. 56, no. 10, pp. 2356–2365, Oct. 2008.

[12] K. Aquilina, M. Thoresen, E. Chakkarapani, I. K. Pople, H. B. Coakham, R. J. Edwards, “Preliminary evaluation of a novel intraparenchymal capacitive intracranial pressure monitor,” *J. Neurosurg.*, vol. 115, no. 3, pp. 561–569, May 2011.

[13] L. Y. Chen, B. C.-K. Tee, A. L. Chortos et al., “Continuous wireless pressure monitoring and mapping with ultra-small passive sensors for health monitoring and critical care,” *Nature Commun.*, vol. 5, article 5028, 2014.

[14] Mohammad H. Behfar, E. Moradi, T. Björninen, L. Sydänheimo, L. Ukkonen, “Biotelemetric wireless intracranial pressure monitoring: an in vitro study,” *Intl. J. Antennas Propag.*, vol. 2015, article ID 918698, Nov. 2015.

[15] M. W. A. Khan, T. Björninen, L. Sydänheimo, and L. Ukkonen, “Characterization of Two-Turns External Loop Antenna With Magnetic Core for Efficient Wireless Powering of Cortical Implants”, *IEEE Antennas And Wireless Propagation Letters*, vol. 15, pp. 1410 – 1414, 2016.

[16] M. W. A. Khan, L. Sydänheimo, L. Ukkonen, T. Björninen, “Inductively powered pressure sensing system integrating a far-field data transmitter for monitoring of intracranial pressure,” *IEEE Sensors Journal*, vol. 17, no. 7, pp. 2191-2197, Apr. 2017.

[17] T. S. Chandrasekar Rao, K. Geetha, “Categories, Standards and Recent Trends in Wireless Power Transfer: A Survey”, *Indian Journal of Science and Technology*, Vol 9(20), DOI: 10.17485/ijst/2016/v9i20/91041, May 2016.

[18] P. Worgan, L. Clare,P. Proynov, B. H. Stark, D. Coyle, “Inductive Power Transfer for On-body Sensors”, *10th EAI International Conference on Pervasive Computing Technologies for Healthcare*, Cancun, Mexico, pp. 16-19, May 2016,.

[19] H. Young and R. Freedman, University Physics. Addison-Wesley, 2004.

[20] Li Qifan, “An inductive power transfer system with a high-q resonant tank for portable device charging”, Master’s Thesis, Department of Electrical and Computer Engineering, National University of Singapore, 2015.

[21] J. I. Agbinya, Wireless Power Transfer. Aalborg: River Publishers, 2012.

[22] K. V. Schuylenbergh, R. Puers, “Inductive Powering: Basic Theory and Application to Biomedical Systems”, 2009, ISBN: 978-90-481-2411-4 and e-ISBN: 978-90-481-2412-1.

[23] Harrington, Roger F. (2003). “Introduction to electromagnetic engineering.” Mineola, NY: Dover Publications. p. 56. ISBN 0-486-43241-6.

[24] J. Choi, Y.-H. Ryu, D. Kim, N. Y. Kim, C. Yoon, Y.K. Park, S. Kwon, and Y. Yang, “Design of high efficiency wireless charging pad based on magnetic resonance coupling,” *EuRAD*, pp. 590 – 593, 2012.

[25] S. Hui, “Planar wireless charging technology for portable electronic products and qi,” *The proceeding of the IEEE*, 101 (6), pp. 1290 – 1301, 2013.

[26] S. Cruciani, T. Campi, F. Maradei, and M. Feliziani, “Numerical simulation of wireless power transfer system to recharge the battery of an implanted cardiac pacemaker,” *EMC Europe*, pp. 44 – 47, 2014.

[27] Y.S. Seo, M. Q. Nguyen, Z. Hughes, S. Rao, and J.C. Chiao, “Wireless power transfer by inductive coupling for implantable batteryless stimulators,” *IEEE MTT-S International*, pp. 1 –3, 2012.

[28] Deyle and M. Reynolds, “Powerpack: A wireless power distribution system for wearable devices,” *ISWC*, pp. 91–98, 2008.

[29] J. Jadidian and D. Katabi, “Magnetic mimo: How to charge your phone in your pocket,” *MobiCom*, pp. 495–506, 2014.

[30] O. Jonah, S. Georgakopoulos, & M. Tentzeris, “Wireless power transfer to mobile wearable device via resonance magnetic” *WACON*, pp. 1–3, 2013.

[31] J. Mikkonen, R. Gowrishankar, M. Oksanen, H. Raittinen, and A. Kolinummi, “OJAS: Open source bi-directional inductive power link,” *ACM CHI*, pp. 1049 – 1058, 2014.

[32] K. Fotopoulou and B. W. Flynn, “Wireless Powering of Implanted Sensors using RF Inductive Coupling”, *IEEE SENSORS 2006, EXCO, Daegu, Korea*, October 22 – 25, 2006.

[33] W. R. Smythe, Static and Dynamic Electricity, 2nd ed., G. P. Harnwell, Ed. New York: McGraw-Hill Book Company, Inc., 1950.

[34] K Singh, “Biotelemetry: could technological developments assist healthcare in rural India”, *The International Electronic Journal of Rural and Remote Health Research, Education*, Practice and Policy, ISSN: 1445-6354, May 2005. Available at: http://rrh.deakin.edu.au.

[35] S. Ramo, J. R. Whinnery, and T. V. Duzer, Fields and Waves in Communication Electronics, 3rd Ed. New York: John Wiley & Sons, Inc., 1994.

[36] S. F. Pichorim and P. J. Abatti, "Design of coils for millimeter and sub-millimeter sized biotelemetry," *IEEE Trans. Biomed. Eng.*, vol. 51, no. 8, pp. 1487 - 1489, 2004.

[37] E. Moradi, K. Koski, T. Björninen, L. Sydänheimo, J. M. Rabaey, J. M. Carmena, Y. Rahmat-Samii, and L. Ukkonen, "Miniature Implantable and Wearable On-Body Antennas: Towards the New Era of Wireless Body-Centric Systems", *IEEE Antennas and Propagation Magazine*, vol. 56, no. 1, pp. 271 – 292, February 2014.

[38] M. W. A. Khan, T. Björninen, L. Sydänheimo, and L. Ukkonen, "Remotely Powered Piezoresistive Pressure Sensor: Toward Wireless Monitoring of Intracranial Pressure", *IEEE Microwave and Wireless Components Letters*, vol.26, no. 7, pp. 549 – 551, July 2016

[39] M. Zargham and P. G. Gulak, "Maximum Achievable Efficiency in Near-Field Coupled Power Transfer Systems," *IEEE Transactions on Biomedical Circuits and Systems*, 6, 3, pp. 228-245, January 2012.

[40] M. Mark et al., "Wireless channel characterization for mm-size neural implants," in Proc. *IEEE EMBS*, Buenos Aires, Argentina, pp. 1565–1568, Aug. 2010.

[41] S. Gabriel, R. W. Lau, and C. Gabriel, "The dielectric properties of biological tissues: III. parametric models for the dielectric spectrum of tissues," *Phys. Med. Biol.*, vol. 41, no. 11, pp. 2271–2293, Nov. 1996.

[42] E. Moradi, T. Björninen, L. Sydänheimo, L. Ukkonen, and J. M. Rabaey, "Analysis of wireless powering of mm-size neural recording tags in RFID inspired wireless brain-machine interface systems," in Proc. *IEEE RFID Conf.*, pp. 8–15, May 2013.

[43] Sun. J, Hynynen K (2013-08-12), "Focusing of therapeutic ultrasound through a human skull: a numerical study", *J Acoust Soc Am*. 104 (3 Pt 1): 1705 – 1715. Bibcode:1998ASAJ..104.1705S. doi:10.1121/1.424383. PMID 9745750.

[44] R. Sarpeshkar, Ultra low power bioelectronics: fundamentals, biomedical applications, and bio-inspired systems, Cambridge University Press, UK, 2010.

[45] R. S. Carson, *High-frequency amplifier*, John Wiley & Sons, USA, 1975.

[46] E. Moradi, S. Amendola, T. Björninen, L. Sydänheimo, J. M. Carmena, J. M. Rabaey, and L. Ukkonen, "Backscattering Neural Tags for Wireless Brain-Machine Interface Systems", *IEEE Transactions On Antennas And Propagation*, vol. 63, no. 2, pp. 719 – 727, February 2015.

[47] T. Björninen, R. Muller, P. Ledochowitsch, L. Sydänheimo, L. Ukkonen, M. M. Maharbiz, and J. M. Rabaey, "Design of Wireless Links to Implanted Brain–Machine Interface Microelectronic Systems", *IEEE Antennas and Wireless Propagation Letters*, vol. 11, pp. 1663-1666, 2012.

[48] E. Moradi, K. Koski, T. Björninen, L. Sydänheimo, J. M. Rabaey, J. M. Carmena, Y. R. Samii, and L. Ukkonen, “Miniature Implantable and Wearable On-Body Antennas: Towards the New Era of Wireless Body-Centric Systems”, *IEEE Antennas and Propagation Magazine*, vol. 56, no. 1, pp. 271-291, 2014.

[49] A. Drossos, V. Santomaa, and N. Kuster, “The Dependence of Electromagnetic Energy Absorption Upon Human Tissue Composition in the Frequency Range of 300-3000 MHz”, *IEEE transactions on microwave theory and techniques*, vol. 48, no. 11, pp. 1988 - 1995, November 2000.

[50] H. A. M. Mahinda, O. P. Murty, “Variability in thickness of human skull bones and sternum – An autopsy experience”, *Journal of Forensic Medicine and Toxicity (International Edition)*, vol. XXVI, no. 2, pp. 26 – 31, Online ISSN 0974-4568, July - December 2009.

[51] Sadler, Thomas W. (February 2009). Langman's Medical Embryology. Lippincott Williams & Wilkins. p. 173. ISBN 0781790697.

[52] M. Waheed Rana, *Human Embryology Made Easy*, Harwood academic publishers, USA, 1998. ISBN: 90-5702-545-0.

[53] RF tools, “LC impedance matching network designer”, Available at: http://leleivre.com/rf_lcmatch.html. [Citation date: 15.3.2017].

APPENDIX A: MATCHING CIRCUIT

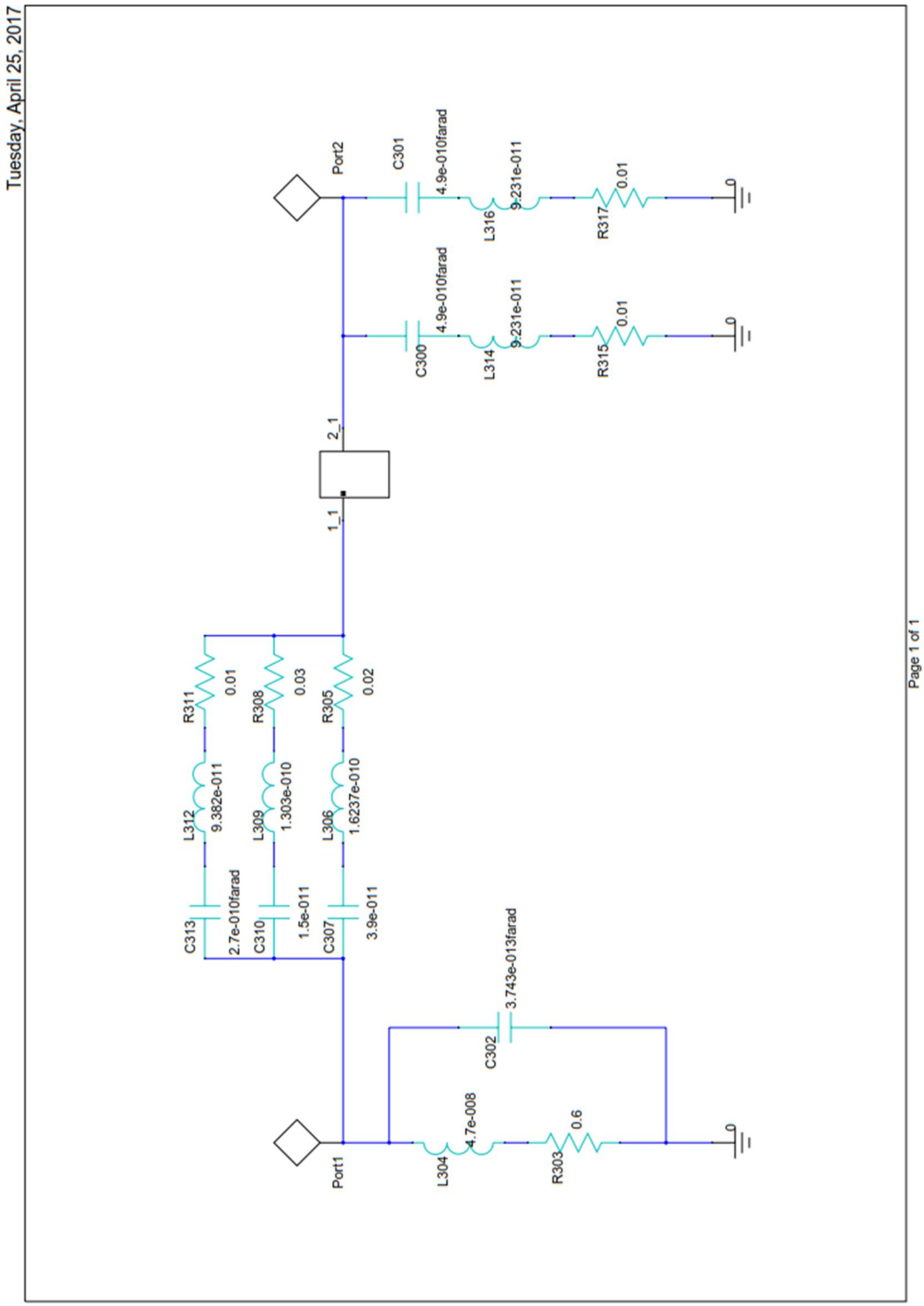

Figure A1: *Matching network of overall system.*

The value of capacitance and inductance are 318.5 pF and 50.44 nH. However, these values are not directly available in laboratory. For this reason, nearest possible values are used. Instead of 318.5 pF and 50.44 nH, closest values of 324 pF and 47 nH are used respectively. Three capacitors of 270 pF, 15 pF, and 39 pF are connected in parallel and act as an equivalent of 324 pF. In practical use, an inductor has some capacitors in parallel and resistor in series as a parasitic element. Similarly, when a capacitor is used, it has some parasitic elements such as inductor and resistance in series. In the Figure C1, inductor 47 nH has 0.6 Ω in series and 0.3743 pF in parallel. The value of 0.3743 pF can be calculated by the resonance frequency equation. Similar procedure is followed for capacitor. Two parallel capacitors of 490 pF are used. 92.31 pH and 10 mΩ are parasitic elements; those are connected in series with 490 pF. The box in between two matching circuit is called N-port network according to simulation. The result for a specific model is imported to this port for analysis of scattering (S) parameter of the network.

Table A1: *Internal resistance and inductance calculations of capacitor, form the data sheets, used in matching circuit.*

Capacitor value (pF)	Series	Equivalent series resistance (ESR) (mΩ)	Series resonance frequency (GHz)	Inductance (pH)
270	1111S42E	18	1	98.82
15	0603	34	3.6	130.30
39	0603	25	2	162.37
560	1111S42E	10	0.7	92.31

Calculation of inductor's parasitic elements:

Operating frequency, f = 15 MHz

Resonance frequency of 47 nH, f_r = 1200 MHz

R_{DC} = 1 Ω (maximum)

Using the equation of resonance frequency, $f_r = \frac{1}{2\pi\sqrt{LC}}$.

Capacitor part of parasitic elements, C = 0.3743 pF.